Match-up database Analyses Report

SMOS-L2-DPGS-v662

Argo

Global Ocean

prepared by the Pi-MEP Consortium

March 05, 2020

Contents

List of Figures

Acronym

Aquarius	NASA/CONAE Salinity mission
ASCAT	Advanced Scatterometer
ATBD	Algorithm Theoretical Baseline Document
BLT	Barrier Layer Thickness
CMORPH	CPC MORPHing technique (precipitation analyses)
CPC	Climate Prediction Center
CTD	Instrument used to measure the conductivity, temperature, and pressure of seawater
DM	Delayed Mode
EO	Earth Observation
ESA	European Space Agency
FTP	File Transfer Protocol
GOSUD	Global Ocean Surface Underway Data
GTMBA	The Global Tropical Moored Buoy Array
Ifremer	Institut français de recherche pour l'exploitation de la mer
IPEV	Institut polaire français Paul-Émile Victor
IQR	Interquartile range
ISAS	*In Situ* Analysis System
Kurt	Kurtosis (fourth central moment divided by fourth power of the standard deviation)
L2	Level 2
LEGOS	Laboratoire d'Etudes en Géophysique et Océanographie Spatiales
LOCEAN	Laboratoire d'Océanographie et du Climat : Expérimentations et Approches Numériques
LOPS	Laboratoire d'Océanographie Physique et Spatiale
MDB	Match-up Data Base
MEOP	Marine Mammals Exploring the Oceans Pole to Pole
MLD	Mixed Layer Depth
NCEI	National Centers for Environmental Information
NRT	Near Real Time
NTAS	Northwest Tropical Atlantic Station
OI	Optimal interpolation
Pi-MEP	Pilot-Mission Exploitation Platform
PIRATA	Prediction and Researched Moored Array in the Atlantic
QC	Quality control
R_{sat}	Spatial resolution of the satellite SSS product
RAMA	Research Moored Array for African-Asian-Australian Monsoon Analysis and Prediction
r^2	Square of the Pearson correlation coefficient
RMS	Root mean square
RR	Rain rate
SAMOS	Shipboard Automated Meteorological and Oceanographic System
Skew	Skewness (third central moment divided by the cube of the standard deviation)
SMAP	Soil Moisture Active Passive (NASA mission)
SMOS	Soil Moisture and Ocean Salinity (ESA mission)
SPURS	Salinity Processes in the Upper Ocean Regional Study
SSS	Sea Surface Salinity
SSS_{insitu}	*In situ* SSS data considered for the match-up

SSS_{SAT}	Satellite SSS product considered for the match-up
ΔSSS	Difference between satellite and *in situ* SSS at colocalized point (ΔSSS = SSS_{SAT}- SSS_{insitu})
SST	Sea Surface Temperature
Std	Standard deviation
Std*	Robust Standard deviation = median(abs(x-median (x)))/0.67 (less affected by outliers than Std)
Stratus	Surface buoy located in the eastern tropical Pacific
Survostral	SURVeillance de l'Océan AuSTRAL (Monitoring the Southern Ocean)
TAO	Tropical Atmosphere Ocean
TSG	ThermoSalinoGraph
WHOI	Woods Hole Oceanographic Institution
WHOTS	WHOI Hawaii Ocean Time-series Station
WOA	World Ocean Atlas

1 Overview

In this report, we present systematic analyses of the Match-up DataBase (MDB) files generated by the Pi-MEP platform within the following Pi-MEP region and for the below pair of Satellite/*in situ* SSS data:

- Pi-MEP region: Global Ocean (download the corresponding mask here)
- SSS satellite product (SSS_{SAT}): SMOS-L2-DPGS-v662
- *In situ* dataset (SSS_{Insitu}): Argo (download the corresponding *in situ* report here)

In the following, ΔSSS= SSS_{SAT}- SSS_{Insitu} denotes the difference between the satellite and *in situ* SSS at the colocalized points that form the MDB.

This report presents successively:

The MDB file DataSets (Section 2)

- A short description of the satellite SSS product considered in the match-up (2.1)
- A short description of the *in situ* SSS dataset considered in the match-up (2.2)
- A short description of the auxiliary geophysical datasets co-localized with SSS pairs (2.3)
- An overview of how the Match-ups were evaluated (2.4)
- An overview of the MDB characteristics for the particular *in situ*/satellite pairs (2.5)

The major results of the MDB file Analyses (Section 3)

- Spatial Maps of the Time-mean and temporal Std of *in situ* and satellite SSS and of the ΔSSS (3.1.1)
- Time series of the monthly median and Std of *in situ* and satellite SSS and of the ΔSSS (3.2)
- Zonal mean and Std of *in situ* and satellite SSS and of the ΔSSS (3.3)
- Scatterplots of satellite vs *in situ* SSS by latitudinal bands (3.4)
- Time series of the monthly median and Std of the ΔSSS sorted by latitudinal bands (3.5)
- ΔSSS sorted as function of geophysical parameters (3.6)
- ΔSSS maps and statistics for different geophysical conditions (3.7)

All analyses are conducted over the Pi-MEP Region specified above and over the full satellite SSS product period. Original figures appearing in this report can be downloaded here as PNG files.

2 The MDB file datasets

2.1 Satellite SSS product

2.1.1 SMOS-L2-DPGS-v662

Quality and major features of the SMOS Level 2 Sea Surface Salinity data products generated by version 662 of the Level 2OS Operational Processor (L2OS) can be found in the SMOS-Level-2-Ocean-Salinity-v662-release-note. Version 662 of the Level 2 Sea Surface Salinity data product is available for the SMOS mission lifetime with the following file class and version:

File class	File version	From	To
REPR	V662	1 June 2010	09 May 2017
OPER	V662	10 May 2017	present

The data set acquired during the SMOS mission commissioning phase (from January 2010 to 31 May 2010) has been acquired during periods when the MIRAS instrument underwent several tests and was operated in different modes, causing drifts not fully compensated by the on-ground calibration processing. For that reason, this data set has not been reprocessed with the latest version of the L2OS processor. The SMOS data users are invited to use this new data set, which supersedes the previous one generated by the algorithm baseline version 622 and to read this note carefully to ensure optimum exploitation of the version 662 data set. Further information on the quality of the data set can be found in the reprocessing reports for data quality control available here and for data verification available here.

Main improvements in the L2OS version 662 data set

The major improvements introduced in the currently operational version 662 of the SMOS Level 2 sea surface salinity processor are:

1. Modified User Data Product (UDP) containing salinities retrieved using only the roughness model previously known as model 1, or SSS1, which has now been selected as the reference model for estimating the sea roughness contribution to brightness temperature. Salinities retrieved using roughness models 2 and 3 are still available in the Data Analysis Product (DAP).

2. A new salinity product corrected for land-sea contamination (LSC) (SSS_corr). Contamination of L1 brightness temperatures when the instrument images a scene that includes a land-sea transition in the FOV (up to 1000 km from the coast) has been shown to introduce significant errors (up to 2 pss) in salinity fields. For a full description, see Annex 5 in the Algorithm Theoretical Baseline Document (ATBD), available here. Bias correction LUTs (so called mixed-scene LUTs) have been generated from a long time series of L1 data for both ascending and descending orbits and are applied to L1 brightness temperatures before retrieval of SSS_corr. The method used to derive the se land-sea contamination correction LUTs is described in section 2.2.8 of the Table Generation Requirement Document (TGRD), available here. If land-sea contamination correction has been applied to any of the measurements used during SSS_corr retrieval, a flag (Fg_ctrl_mixed_scene) is set. Salinities retrieved without land-sea correction (SSS_uncorr) are also available in the UDP.

3. New (experimental) salinity anomaly product (SSS_anom) computed from SSS_corr and WOA 2009 climatology (SSS_anom = SSS_corr minus WOA 2009). Daily interpolated climatology is computed from the monthly WOA 2009 LUT before extracting SSS_anom.

ESL s plan to develop a SMOS-based climatology to be used in future versions of the L2OS processor, with the objective of providing a de-biased SSS anomaly field.

4. New scene-based filtering algorithm to mitigate contamination from RFI and other sources (e.g., sun), based on a set of metrics comparing differences between brightness temperatures of successive snapshots including a complete polarization cycle (so-called scenes). A scene is defined in section 2.2.8.2 of the TGRD, and the scene-based filtering algorithm is described in section 2.2.8.4 of the TGRD, available here.

5. New sun glint model and sun brightness temperatures LUTs used as part of the forward model, and to set sun glint flags more accurately. Operational (OPER) products use a constant sun brightness temperature, whereas the reprocessed products (REPR) use a daily estimated L-band sun brightness temperature LUT for orbits prior to 22 November 2016.

6. Roughness model 1 LUT has been updated by ESL, improving the estimation of forward model roughness brightness temperatures at wind speeds > 12 m/s.

7. TEC retrieved from SMOS 3rd Stokes polarimetric measurements used for both ascending and descending orbits (for both sea surface salinity retrievals and OTT computation), to provide an improved Faraday rotation estimation.

8. Acard parameter computed with land-sea corrected L1 brightness temperatures and the complete forward model including flat sea, roughness model 1, galactic and sun glint components.

9. Modified UDP format : see Tables below. Land sea contamination corrected salinities and associated fields/flags have suffix "_corr"; uncorrected salinities have suffix "_uncorr"; whilst anomalies have suffix "_anom". For further details of the new UDP format see tables 47, 48 and 49 in section 3.2.6 of the Input/Output Data Definition Document (IODD) available here.

10. Updated configuration of switches and filters used in the data processing. For further information see the section 2.4.7 of the TGRD, available here. The L2OS version 662 data set has been generated using the same L1c data set as the previous L2OS version 622 data set: i.e., L1c data version 620. For further details on the L1c data sets see the L1c data version 620 read-me-first note available here: here

L2OS version 662 performance and caveats

The reprocessed data set has been analysed by ESLs and ARGANS. The reference document is mentioned above. The main conclusions are:

- Land-sea contamination corrected salinities (SSS_corr) almost cancel the global mean bias in near -to-coast regions (> 40 km and < 800 km) compared to SSS_uncorr. Also, there are more valid SSS_corr retrievals near to the coast than in SSS_uncorr (the LSC correction allows retrieval of previously contaminated pixels). However, in regions with high RFI (e.g. China seas, NW Indian Ocean, DEW line - see RFI probability maps from CESBIO: `http://www.cesbio.upstlse.fr/SMOS_blog/smos_rfi/`) or natural geophysical variability (e.g. river plumes), land-sea contamination correction is either unavailable (due to insufficient data to compute the land-sea correction LUT) or unreliable (due to a mismatch between WOA climatology and rapid salinity variability). In these regions, SSS_corr is prone to inaccuracies (see also plots in Section 5 below).

- Globally, the novel scene-based filtering and updated roughness model 1 determine an increase in the number of retrievals in both ascending and descending orbits. The new sun glint model also allows an increase in the number and quality of retrievals at the edge of the swath during periods of high sun glint (e.g., western edge of southern hemisphere descending orbits, in November-January) and high sun L-band intensity (2012-2015).
- The new experimental salinity anomaly product is still experimental, as the WOA 2009 climatology is not always directly related to SMOS surface salinities, especially in regions of high variability (e.g., ITCZ). ESLs plan to derive a SMOS based climatology for future anomaly products, to provide a field intrinsically devoid of systematic errors. The El-Niño event of 2015-2016 is visible in Pacific region ascending and descending orbit Hovmoller plots (see Section 2.4.1 in the L2OS v662 reprocessing verification report).
- Across-track biases and ascending-descending differences still remain. Retrievals near to the edge of the swath (x_swath > ± 350 km) have higher uncertainties due to the smaller number of measurements, and contamination from various sources, especially sun aliases and associated ripples (tails). Ascending orbits have less bias than descending (see across-track Hovmoller plots in the L2OS v662 reprocessing verification report), while descending passes have stronger biases during January March and October-December periods.
- ESLs have reported that there is evidence of residual inaccuracies in salinity retrievals due to TEC and galactic glint modelling issues. Therefore, users should be aware that salinities retrieved during periods of high TEC activity (corresponding to high solar activity, especially for descending orbits) and high galactic glint (see sections 5.2 and 5.5 in the L2OS Reprocessing Report) are less accurate.
- Strong latitudinal bias in SSS_corr can be seen in the Northern Hemisphere during March-May in both ascending and descending orbits (see global Hovmoller plots in figures 18 and 20 in the L2OS v662 re processing verification report), but these are not visible in SSS_uncorr. Similar latitudinal biases can also be seen in SSS_anom for Pacific and Atlantic regions (see Hovmoller plots in figures 35-39 in the L2OS v662 reprocessing report). Therefore, land-sea contamination corrected salinities (and anomalies) above 30N during these periods exhibit worse performance than elsewhere or in different periods of the year.

Filtering retrievals

We strongly recommend users to filter L2OS sea surface salinity retrievals using one of the following set of criteria:

1. For best quality data: Dg_quality_SSS < 150
2. For more data but with lower quality : Fg_ctrl_poor_geophysical = 0 and Fg_ctrl_poor_retrieval = 0
3. Other combinations of UDP flags and filters including at least Fg_ctrl_chi2 = 0 or Fg_ctrl_chi2_P = 0
4. Other filters used by the L2OS Expert Support Laboratories for generating Level 3 salinity maps as described in the L2OS v662 reprocessing verification report sections 2.1 and 2.2, available here.

Flags used before MDB files generation
We only select data in the MDB files such as the following conditions or flags are met:

- Dg_quality_SSS < 150
- Dg_af_fov > 130
- control_flag_set: CTRL_ECMWF
- control_flag_clear: CTRL_NUM_MEAS_MIN, CTRL_NUM_MEAS_LOW, CTRL_MANY_OUTLIERS, CTRL_SUNGLINT, CTRL_MOONGLINT, CTRL_REACH_MAXITER, CTRL_MARQ, CTRL_CHI2_P, CTRL_SUSPECT_RFI
- science_flag_set: SC_LOW_WIND, SC_LAND_SEA_COAST1
- science_flag_clear: SC_ICE, SC_SUSPECT_ICE

Satellite SSS product characteristics

Table 1: Satellite SSS product characteristics

SMOS-L2-DPGS-v662	
Spatial resolution	~40 km
Temporal repeat	3 days
Temporal coverage	From 2010-06-01 to now
Spatial coverage	Global [-180 180 -90 90]
Data Provider	ESA
Version	662
ATBD	SMOS_L2OS-ATBD
Data access	level-2-ocean-salinity

2.2 *In situ* SSS dataset

Argo is a global array of 3,000 free-drifting profiling floats that measures the temperature and salinity of the upper 2000 m of the ocean. This allows continuous monitoring of the temperature and salinity of the upper ocean, with all data being relayed and made publicly available within hours after collection. The array provides around 100,000 temperature/salinity profiles per year distributed over the global oceans at an average of 3-degree spacing. Only Argo salinity and temperature float data with quality index set to 1 or 2 and data mode set to real time (RT), real time adjusted (RTA) and delayed mode (DM) are considered in the Pi-MEP. Argo floats which may have problems with one or more sensors appearing in the grey list maintained at the Coriolis/GDACs are discarded. Furthermore, Pi-MEP provides an additional list of ~1000 "suspicious" argo salinity profiles that are also removed before analysis. The upper ocean salinity and temperature values recorded between 0m and 10m depth are considered as Argo sea surface salinities (SSS) and sea surface temperatures (SST). These data were collected and made freely available by the international Argo project and the national programs that contribute to it (Argo (2000)).

2.3 Auxiliary geophysical datasets

Additional EO datasets are used to characterize the geophysical conditions at the *in situ*/satellite SSS pair measurement locations and time, and 10 days prior the measurements to get an estimate of the geophysical condition and history. As discussed in Boutin et al. (2016), the presence of vertical gradients in, and horizontal variability of, sea surface salinity indeed complicates comparison of satellite and *in situ* measurements. The additional EO data are used here to get a first estimates of conditions for which L-band satellite SSS measured in the first centimeters of the upper ocean within a 50-150 km diameter footprint might differ from pointwise *in situ* measurements performed in general between 10 and 5 m depth below the surface. The spatio-temporal variability of SSS within a satellite footprint (50–150 km) is a major issue for satellite SSS validation in the vicinity of river plumes, frontal zones, and significant precipitation. Rainfall can in some cases produce vertical salinity gradients exceeding 1 pss m^{-1}; consequently, it is recommended that satellite and *in situ* SSS measurements less than 3–6 h after rain events should be considered with care when used in satellite calibration/validation analyses. To identify such situation, the Pi-MEP platform is first using CMORPH products to characterize the local value and history of rain rate and ASCAT gridded data are used to characterize the local surface wind speed and history. For validation purpose, the ISAS monthly SSS *in situ* analysed fields at 5 m depth are collocated and compared with the satellite SSS products. The use of ISAS is motivated by the fact that it is used in the SMOS L2 official validation protocol in which systematic comparisons of SMOS L2 retrieved SSS with ISAS are done. In complement to ISAS, monthly std climatological fields from the World Ocean Atlas (WOA13) at the match-up pairs location and date are also used to have an a priori information of the local SSS variability.

2.3.1 CMORPH

Precipitation are estimated using the CMORPH 3-hourly products at 1/4° resolution (Joyce et al. (2004)). CMORPH (CPC MORPHing technique) produces global precipitation analyses at very high spatial and temporal resolution. This technique uses precipitation estimates that have been derived from low orbiter satellite microwave observations exclusively, and whose features are transported via spatial propagation information that is obtained entirely from geostationary satellite IR data. At present NOAA incorporate precipitation estimates derived from the passive microwaves aboard the DMSP 13, 14 and 15 (SSM/I), the NOAA-15, 16, 17 and 18 (AMSU-B), and AMSR-E and TMI aboard NASA's Aqua, TRMM and GPM spacecraft, respectively. These estimates are generated by algorithms of Ferraro (1997) for SSM/I, Ferraro et al. (2000) for AMSU-B and Kummerow et al. (2001) for TMI. Note that this technique is not a precipitation estimation algorithm but a means by which estimates from existing microwave rainfall algorithms can be combined. Therefore, this method is extremely flexible such that any precipitation estimates from any microwave satellite source can be incorporated.

With regard to spatial resolution, although the precipitation estimates are available on a grid with a spacing of 8 km (at the equator), the resolution of the individual satellite-derived estimates is coarser than that - more on the order of 12 x 15 km or so. The finer ”resolution” is obtained via interpolation.

In effect, IR data are used as a means to transport the microwave-derived precipitation features during periods when microwave data are not available at a location. Propagation vector matrices are produced by computing spatial lag correlations on successive images of geostationary satellite IR which are then used to propagate the microwave derived precipitation estimates. This process governs the movement of the precipitation features only. At a given location, the shape and intensity of the precipitation features in the intervening half hour periods between microwave scans are determined by performing a time-weighting interpolation between microwave-derived features that have been propagated forward in time from the previous microwave observation and those that have been propagated backward in time from the following microwave scan. NOAA refer to this latter step as "morphing" of the features.

For the present Pi-MEP products, we only considered the 3-hourly products at 1/4 degree resolution. The entire CMORPH record (December 2002-present) for 3-hourly, 1/4 degree lat/lon resolution can be found at: `ftp://ftp.cpc.ncep.noaa.gov/precip/CMORPH_V1.0/CRT/`. CMORPH estimates cover a global belt (-180°W to 180°E) extending from 60°S to 60°N latitude and are available for the complete period of the Pi-MEP core datasets (Jan 2010-now).

2.3.2 ASCAT

Advanced SCATterometer (ASCAT) daily data produced and made available at Ifremer/CERSAT on a 0.25°x0.25° resolution grid (Bentamy and Fillon (2012)) since March 2007 are used to characterize the mean daily wind at the match-up pair location as well as the wind history during the 10-days period preceding the in situ measurement date. These wind fields are calculated based on a geostatistical method with external drift. Remotely sensed data from ASCAT are considered as observations while those from numerical model analysis (ECMWF) are associated with the external drift. The spatial and temporal structure functions for wind speed, zonal and meridional wind components are estimated from ASCAT retrievals. Furthermore, the new procedure includes a temporal interpolation of the retrievals based on the complex empirical orthogonal function (CEOF) approach, in order to enhance the sampling length of the scatterometer observations. The resulting daily wind fields involves the main known surface wind patterns as well as some variation modes associated with temporal and spatial moving features. The accuracy of the gridded winds was investigated through comparisons with moored buoy data in Bentamy et al. (2012) and resulted in rms differences for wind speed and direction are about 1.50 m.s^{-1} and 20°.

2.3.3 ISAS

The In Situ Analysis System (ISAS), as described in Gaillard et al. (2016) is a data based reanalysis of temperature and salinity fields over the global ocean. It was initially designed to synthesize the temperature and salinity profiles collected by the Argo program. It has been later extended to accommodate all type of vertical profile as well as time series. ISAS gridded fields are entirely based on *in situ* measurements. The methodology and configuration have been conceived to preserve as much as possible the data information content and resolution. ISAS is developed and run in a research laboratory (LOPS) in close collaboration with Coriolis, one of Argo Global Data Assembly Center and unique data provider for the Mercator operational oceanography system. At the moment the period covered starts in 2002 and only the upper 2000 m are considered. The gridded fields were produced over the global ocean 70°N–70°S on a 1/2° grid by the ISAS project with datasets downloaded from the Coriolis data center (for more details on ISAS see Gaillard et al. (2009)). In the Pi-MEP, the product in used is the INSITU_GLO_TS_OA_NRT_OBSERVATIONS_013_002_a v6.2 NRT derived at the Coriolis data center and provided by the Copernicus Marine Environment Monitoring Service (CMEMS). The major contribution to the data set is from Argo array of profiling floats, reaching an approximate resolution of one profile every 10-days and every 3-degrees over the satellite SSS period (`http://www.umr-lops.fr/SNO-Argo/Products/ISAS-T-S-fields/`); in this version SSS from ship of opportunity thermosalinographs are not used, so that we can consider SMOS SSS validation using these measurements independent of ISAS. The ISAS optimal interpolation involves a structure function modeled as the sum of two Gaussian functions, each associated with specific time and space scales, resulting in a smoothing over typically 3 degrees. The smallest scale which can be retrieved with ISAS analysis is not smaller than 300–500 km (Kolodziejczyk et al. (2015)). For validation purpose, the ISAS monthly SSS fields at 5 m depth are collocated and compared with the satellite SSS products and included in the Pi-MEP Match-up files. In addition, the "percentage of variance" fields (PCTVAR) contained in the ISAS analyses provide information on the local variability of *in situ* SSS measurements within 1/2°x1/2° boxes.

2.3.4 World Ocean Atlas Climatology

The World Ocean Atlas 2013 version 2 (WOA13 V2) is a set of objectively analyzed (1° grid) climatological fields of *in situ* temperature, salinity and other variables provided at standard depth levels for annual, seasonal, and monthly compositing periods for the World Ocean. It also includes associated statistical fields of observed oceanographic profile data interpolated to standard depth levels on 5°, 1°, and 0.25° grids. We use these fields in complement to ISAS to characterize the climatological fields (annual mean and std) at the match-up pairs location and date.

2.4 Overview of the Match-ups generation method

The match-up production is basically a three steps process:

1. preparation of the input *in situ* and satellite data, and,
2. co-localization of satellite products with *in situ* SSS measurements.
3. co-localization of the *in situ*/satellite pair with auxiliary information.

In the following, we successively detail the approaches taken for these different steps.

2.4.1 *In situ*/Satellite data filtering

The first step consists in filtering Argo *in situ* data using the quality flags as described in 2.2 so that only valid salinity data remains in the final match-up files.

For high-spatial resolution *in situ* SSS measurements such as the Thermo-SalinoGraph (TSG) SSS data from research vessels, Voluntary Observing Ships (VOS) or sailing ships, as well as SSS data from surface drifters, an additional spatial filtering step is performed on the *in situ* data that will be in fine compared to the satellite SSS products. If R_{sat} is the spatial resolution of the satellite SSS product (L2 to L3-L4), the *in situ* data at its original spatial resolution are spatially low pass filtered using a running median filter with a window width=R_{sat} in order to try to minimize the spatial representativeness uncertainty when comparing to the lower spatial resolution of the satellite SSS product. Both original and filtered data are finally stored in the MDB files.

Only for satellite L2 SSS data, a third step consist in filtering spurious data using the flags and associated recommendation as provided by the official data centers and described in 2.1.

2.4.2 *In situ*/Satellite Co-localization

In this step, each SSS satellite acquisition is co-localized with the filtered *in situ* measurements. The method used for co-localization differ if the satellite SSS is a swath product (so-called Level 2-types) or a time-space composite product (so-called Level 3/level 4-types).

- For L2 SSS swath data :

  If R_{sat} is the spatial resolution of the satellite swath SSS product, for each *in situ* data sample collected in the Pi-MEP database, the platform searches for all satellite SSS data found at grid nodes located within a radius of $R_{sat}/2$ from the *in situ* data location and acquired with a time-lag from the *in situ* measurement date that is less or equal than ± 12 hours. If several satellite SSS samples are found to meet these criteria, the final satellite SSS match-up point is selected to be the closest in time from the *in situ* data measurement date. The final spatial and temporal lags between the *in situ* and satellite data are stored in the MDB files.

- For L3 and L4 composite SSS products :

  If R_{sat} is the spatial resolution of the composite satellite SSS product and D the period over which the composite product was built (e.g., periods of 1, 7, 8, 9, 10, 18 days, 1 month, etc..) with central time t_o, for each *in situ* data sample collected in the Pi-MEP database during period D, the platform searches for all satellite SSS data of the composite product found at grid nodes located within a radius of $R_{sat}/2$ from the *in situ* data location. If several satellite SSS product samples are found to meet these criteria, the final satellite SSS match-up point is chosen to be the composite SSS with central time t_o which is the closest in time from the *in situ* data measurement date. The final spatial and temporal lags between the *in situ* and satellite data are stored in the MDB files.

2.4.3 MDB pair Co-localization with auxiliary data and complementary information

MDB data consist of satellite and *in situ* SSS pairs but also of auxiliary geophysical parameters such as local and history of wind speed and rain rates, as well as various information (climatology, distance to coast, mixed layer depth, barrier layer thickness, etc) that can be derived from *in situ* data and which are included in the final match-up files. The collocation of auxiliary parameters and additional information is done for each *in situ* SSS measurement contained in the match-up files as follows :

If t_{insitu} is the time/date at which the *in situ* measurement is performed, we collect:

- The ASCAT wind speed product of the same day than t_{insitu} found at the ASCAT 1/4° grid node with closest distance from the *in situ* data location and the time series of the ASCAT wind speed at the same node for the 10 days prior the *in situ* measurement day.

- If the *in situ* data is located within the 60°N-60°S band, we select the CMORPH 3-hourly product the closest in time from t_{insitu} and found at the CMORPH 1/4° grid node with closest distance from the *in situ* data location. We then store the time series of the CMORPH rain rate at the same node for the 10 days prior the *in situ* measurement time.

For the given month/year of the *in situ* data, we select the ISAS and WOA fields for the same month (and same year for ISAS fields) and take the SSS analysis (monthly mean, std) found at the closest grid node from the *in situ* measurement.

The distance from the *in situ* SSS data location to the nearest coast is evaluated and provided in km. We use a distance-to-coast map at 1/4° resolution where small islands have been removed.

When vertical profiles of salinity (S) and temperature (T) are made available from the *in situ* measurements used to build the match-up (Argo or sea mammals), the following variables are included into each satellite/*in situ* match-up file:

1. The vertical distribution of pressure at which the profile were measured,

2. The vertical S(z) and T(z) profiles,

3. The vertical potential density anomaly profile $\sigma_0(z)$,

4. The Mixed Layer Depth (MLD). The MLD is defined here as the depth where the potential density has increased from the reference depth (10 meter) by a threshold equivalent to 0.2°C decrease in temperature at constant salinity: $\sigma_0 = \sigma_{010m} + \Delta\sigma_0$ with $\Delta\sigma_0 = \sigma_0(\theta_{10m} - 0.2, S_{10m}) - \sigma_0(\theta_{10m}, S_{10m})$ where θ_{10m} and S_{10m} are the temperature and salinity at the reference depth (i.e. 10 m) (de Boyer Montégut et al. (2004), de Boyer Montégut et al. (2007)).

5. The Top of the Thermocline Depth (TTD) is defined as the depth at which temperature decreases from its 10 m value by 0.2°C.

6. The Barrier Layer if present, is defined as the intermediate layer between the top of the thermocline and the bottom of the density mixed-layer and its thickness (BLT) is defined as the difference between the MLD and the TTD.

7. The vertical profile of the buoyancy frequency $N^2(z)$

The resulting match-ups files are serialized as NetCDF-4 files whose structure depends on the origin of the *in situ* data they contain and is described in section 2.4.4.

2.4.4 Content of the Match-Up NetCDF files

```
netcdf pimep-mdb_smos-l2-v662_argo_TIMEID_v01 {
dimensions:
        N_prof = 944 ;
        N_LEVELS = 499 ;
        N_DAYS_WIND = 10 ;
        N_3H_RAIN = 80 ;
        TIME_Sat = UNLIMITED ; // (1 currently)
variables:
float DATE_ARGO(N_prof) ;
        DATE_ARGO:long_name = "Date of Argo profile" ;
        DATE_ARGO:units = "days since 1990-01-01 00:00:00" ;
        DATE_ARGO:standard_name = "time" ;
        DATE_ARGO:_FillValue = -999.f ;
float LATITUDE_ARGO(N_prof) ;
        LATITUDE_ARGO:long_name = "Latitude of Argo profile" ;
        LATITUDE_ARGO:units = "degrees_north" ;
        LATITUDE_ARGO:valid_min = -90. ;
        LATITUDE_ARGO:valid_max = 90. ;
        LATITUDE_ARGO:standard_name = "latitude" ;
        LATITUDE_ARGO:_FillValue = -999.f ;
float LONGITUDE_ARGO(N_prof) ;
        LONGITUDE_ARGO:long_name = "Longitude of Argo profile" ;
        LONGITUDE_ARGO:units = "degrees_east" ;
        LONGITUDE_ARGO:valid_min = -180. ;
        LONGITUDE_ARGO:valid_max = 180. ;
        LONGITUDE_ARGO:standard_name = "longitude" ;
```

LONGITUDE_ARGO:_FillValue = -999.f ;
float SSS_DEPTH_ARGO(N_prof) ;
SSS_DEPTH_ARGO:long_name = ”Sea water pressure at Argo float location (equals 0 at sea level)” ;
SSS_DEPTH_ARGO:units = ”decibar” ;
SSS_DEPTH_ARGO:standard_name = ”sea_water_pressure” ;
SSS_DEPTH_ARGO:_FillValue = -999.f ;
float SSS_ARGO(N_prof) ;
SSS_ARGO:long_name = ”Argo SSS” ;
SSS_ARGO:units = ”1” ;
SSS_ARGO:salinity_scale = ”Practical Salinity Scale(PSS-78)” ;
SSS_ARGO:standard_name = ”sea_water_salinity” ;
SSS_ARGO:_FillValue = -999.f ;
float SST_ARGO(N_prof) ;
SST_ARGO:long_name = ”Argo SST” ;
SST_ARGO:units = ”degree Celsius” ;
SST_ARGO:standard_name = ”sea_water_temperature” ;
SST_ARGO:_FillValue = -999.f ;
float DELAYED_MODE_ARGO(N_prof) ;
DELAYED_MODE_ARGO:long_name = ”Argo data mode (delayed mode = 1, real time =0) ” ;
DELAYED_MODE_ARGO:units = ”1” ;
DELAYED_MODE_ARGO:_FillValue = -999.f ;
float DISTANCE_TO_COAST_ARGO(N_prof) ;
DISTANCE_TO_COAST_ARGO:long_name = ”Distance to coasts at Argo float location” ;
DISTANCE_TO_COAST_ARGO:units = ”km” ;
DISTANCE_TO_COAST_ARGO:_FillValue = -999.f ;
float PLATFORM_NUMBER_ARGO(N_prof) ;
PLATFORM_NUMBER_ARGO:long_name = ”Argo float unique identifier” ;
PLATFORM_NUMBER_ARGO:conventions = ”WMO float identifier : A9IIIII” ;
PLATFORM_NUMBER_ARGO:units = ”1” ;
PLATFORM_NUMBER_ARGO:_FillValue = -999.f ;
float PSAL_ARGO(N_prof, N_LEVELS) ;
PSAL_ARGO:long_name = ”Argo salinity profile” ;
PSAL_ARGO:units = ”1” ;
PSAL_ARGO:salinity_scale = ”Practical Salinity Scale (PSS-78)” ;
PSAL_ARGO:standard_name = ”sea_water_salinity” ;
PSAL_ARGO:_FillValue = -999.f ;
float TEMP_ARGO(N_prof, N_LEVELS) ;
TEMP_ARGO:long_name = ”Argo temperature profile” ;
TEMP_ARGO:units = ”degree Celsius” ;
TEMP_ARGO:standard_name = ”sea_water_temperature” ;
TEMP_ARGO:_FillValue = -999.f ;
float PRES_ARGO(N_prof, N_LEVELS) ;
PRES_ARGO:long_name = ”Argo pressure profile” ;
PRES_ARGO:units = ”decibar” ;
PRES_ARGO:standard_name = ”sea_water_pressure” ;
PRES_ARGO:_FillValue = -999.f ;

float RHO_ARGO(N_prof, N_LEVELS) ;
RHO_ARGO:long_name = "Argo in-situ density profile" ;
RHO_ARGO:units = "kg/m" ;
RHO_ARGO:_FillValue = -999.f ;
float SIGMA0_ARGO(N_prof, N_LEVELS) ;
SIGMA0_ARGO:long_name = "Argo potential density anomaly profile" ;
SIGMA0_ARGO:units = "kg/m^3" ;
SIGMA0_ARGO:_FillValue = -999.f ;
float N2_ARGO(N_prof, N_LEVELS) ;
N2_ARGO:long_name = "Argo buoyancy frequency profile" ;
N2_ARGO:units = "1/s^2" ;
N2_ARGO:_FillValue = -999.f ;
float MLD_ARGO(N_prof) ;
MLD_ARGO:long_name = "Mixed Layer Depth (MLD) calculated from Argo profile (depth where $\sigma_0 = \sigma_{010m} + \Delta\sigma_0$ with $\Delta\sigma_0 = \sigma_0(\theta_{10m} - 0.2, S_{10m}) - \sigma_0(\theta_{10m}, S_{10m})$)" ;
MLD_ARGO:units = "m" ;
MLD_ARGO:_FillValue = -999.f ;
float TTD_ARGO(N_prof) ;
TTD_ARGO:long_name = "Top of Thermocline Depth (TTD) calculated from Argo profile (depth where $\theta = \theta_{10m} - 0.2$)" ;
TTD_ARGO:units = "m" ;
TTD_ARGO:_FillValue = -999.f ;
float BLT_ARGO(N_prof) ;
BLT_ARGO:long_name = "Barrier Layer Thickness (TTD-MLD)" ;
BLT_ARGO:units = "m" ;
BLT_ARGO:_FillValue = -999.f ;
float DATE_Satellite_product(TIME_Sat) ;
DATE_Satellite_product:long_name = "Central time of satellite SSS file" ;
DATE_Satellite_product:units = "days since 1990-01-01 00:00:00" ;
DATE_Satellite_product:standard_name = "time" ;
float LATITUDE_Satellite_product(N_prof) ;
LATITUDE_Satellite_product:long_name = "Satellite product latitude at Argo float location" ;
LATITUDE_Satellite_product:units = "degrees_north" ;
LATITUDE_Satellite_product:valid_min = -90. ;
LATITUDE_Satellite_product:valid_max = 90. ;
LATITUDE_Satellite_product:standard_name = "latitude" ;
LATITUDE_Satellite_product:_FillValue = -999.f ;
float LONGITUDE_Satellite_product(N_prof) ;
LONGITUDE_Satellite_product:long_name = "Satellite product longitude at Argo float location" ;
LONGITUDE_Satellite_product:units = "degrees_east" ;
LONGITUDE_Satellite_product:valid_min = -180. ;
LONGITUDE_Satellite_product:valid_max = 180. ;
LONGITUDE_Satellite_product:standard_name = "longitude" ;
LONGITUDE_Satellite_product:_FillValue = -999.f ;
float SSS_Satellite_product(N_prof) ;
SSS_Satellite_product:long_name = "Satellite product SSS at Argo float location" ;
SSS_Satellite_product:units = "1" ;

SSS_Satellite_product:salinity_scale = "Practical Salinity Scale(PSS-78)" ;
SSS_Satellite_product:standard_name = "sea_surface_salinity" ;
SSS_Satellite_product:_FillValue = -999.f ;
float SST_Satellite_product(N_prof) ;
SST_Satellite_product:long_name = "Satellite product SST at Argo float location" ;
SST_Satellite_product:units = "degree Celsius" ;
SST_Satellite_product:standard_name = "sea_surface_temperature" ;
SST_Satellite_product:_FillValue = -999.f ;
float Spatial_lags(N_prof) ;
Spatial_lags:long_name = "Spatial lag between Argo float location and satellite SSS product pixel center" ;
Spatial_lags:units = "km" ;
Spatial_lags:_FillValue = -999.f ;
float Time_lags(N_prof) ;
Time_lags:long_name = "Temporal lag between Argo float time and satellite SSS product central time" ;
Time_lags:units = "days" ;
Time_lags:_FillValue = -999.f ;
float ROSSBY_RADIUS_at_ARGO(N_prof) ;
ROSSBY_RADIUS_at_ARGO:long_name = "Baroclinic Rossby radius of deformation (Chelton et al., 1998) at Argo float location" ;
ROSSBY_RADIUS_at_ARGO:units = "km" ;
ROSSBY_RADIUS_at_ARGO:_FillValue = -999.f ;
float Ascat_daily_wind_at_ARGO(N_prof) ;
Ascat_daily_wind_at_ARGO:long_name = "Daily Ascat wind speed module at Argo float location" ;
Ascat_daily_wind_at_ARGO:units = "m/s" ;
Ascat_daily_wind_at_ARGO:_FillValue = -999.f ;
float CMORPH_3h_Rain_Rate_at_ARGO(N_prof) ;
CMORPH_3h_Rain_Rate_at_ARGO:long_name = "3-hourly CMORPH rain rate at Argo float location" ;
CMORPH_3h_Rain_Rate_at_ARGO:units = "mm/3h" ;
CMORPH_3h_Rain_Rate_at_ARGO:_FillValue = -999.f ;
float Ascat_10_prior_days_wind_at_ARGO(N_prof, N_DAYS_WIND) ;
Ascat_10_prior_days_wind_at_ARGO:long_name = "Prior 10 days time series of Ascat wind speed module at Argo float location" ;
Ascat_10_prior_days_wind_at_ARGO:units = "m/s" ;
Ascat_10_prior_days_wind_at_ARGO:_FillValue = -999.f ;
float CMORPH_10_prior_days_Rain_Rate_at_ARGO(N_prof, N_3H_RAIN) ;
CMORPH_10_prior_days_Rain_Rate_at_ARGO:long_name = "Prior 10 days times series of 3-hourly CMORPH Rain Rate at Argo float location" ;
CMORPH_10_prior_days_Rain_Rate_at_ARGO:units = "mm/3h" ;
CMORPH_10_prior_days_Rain_Rate_at_ARGO:_FillValue = -999.f ;
float SSS_ISAS_at_ARGO(N_prof) ;
SSS_ISAS_at_ARGO:long_name = "ISAS SSS (5m depth) at Argo float location" ;
SSS_ISAS_at_ARGO:units = "1" ;
SSS_ISAS_at_ARGO:salinity_scale = "Practical Salinity Scale(PSS-78)" ;
SSS_ISAS_at_ARGO:standard_name = "sea_water_salinity" ;
SSS_ISAS_at_ARGO:_FillValue = -999.f ;

float SSS_PCTVAR_ISAS_at_ARGO(N_prof) ;
SSS_PCTVAR_ISAS_at_ARGO:long_name = "Error on ISAS SSS (5m depth) at Argo float location (% variance)" ;
SSS_PCTVAR_ISAS_at_ARGO:units = "%" ;
SSS_PCTVAR_ISAS_at_ARGO:_FillValue = -999.f ;
float SSS_WOA13_at_ARGO(N_prof) ;
SSS_WOA13_at_ARGO:long_name = "WOA 2013 (DECAV-1deg) SSS (0m depth) at Argo float location" ;
SSS_WOA13_at_ARGO:units = "1" ;
SSS_WOA13_at_ARGO:salinity_scale = "Practical Salinity Scale(PSS-78)" ;
SSS_WOA13_at_ARGO:standard_name = "sea_surface_salinity" ;
SSS_WOA13_at_ARGO:_FillValue = -999.f ;
float SSS_STD_WOA13_at_ARGO(N_prof) ;
SSS_STD_WOA13_at_ARGO:long_name = "WOA 2013 (DECAV-1deg) SSS STD (0m depth) at Argo float location " ;
SSS_STD_WOA13_at_ARGO:units = "1" ;
SSS_STD_WOA13_at_ARGO:_FillValue = -999.f ;
float SSS_ISAS15_at_ARGO(N_prof) ;
SSS_ISAS15_at_ARGO:long_name = "Monthly ISAS-15 SSS (5m depth) at Argo float location" ;
SSS_ISAS15_at_ARGO:units = "1" ;
SSS_ISAS15_at_ARGO:salinity_scale = "Practical Salinity Scale (PSS-78)" ;
SSS_ISAS15_at_ARGO:standard_name = "sea_water_salinity" ;
SSS_ISAS15_at_ARGO:_FillValue = -999.f ;
float SSS_PCTVAR_ISAS15_at_ARGO(N_prof) ;
SSS_PCTVAR_ISAS15_at_ARGO:long_name = "Error on monthly ISAS-15 SSS (5m depth) at Argo float location (% variance)" ;
SSS_PCTVAR_ISAS15_at_ARGO:units = "%" ;
SSS_PCTVAR_ISAS15_at_ARGO:_FillValue = -999.f ;
float SSS_WOA18_at_ARGO(N_prof) ;
SSS_WOA18_at_ARGO:long_name = "Monthly WOA 2018 (DECAV-1deg) SSS (0m depth) at Argo float location" ;
SSS_WOA18_at_ARGO:units = "1" ;
SSS_WOA18_at_ARGO:salinity_scale = "Practical Salinity Scale (PSS-78)" ;
SSS_WOA18_at_ARGO:standard_name = "sea_surface_salinity" ;
SSS_WOA18_at_ARGO:_FillValue = -999.f ;
float SSS_STD_WOA18_at_ARGO(N_prof) ;
SSS_STD_WOA18_at_ARGO:long_name = "Monthly WOA 2018 (DECAV-1deg) SSS STD (0m depth) at Argo float location " ;
SSS_STD_WOA18_at_ARGO:units = "1" ;
SSS_STD_WOA18_at_ARGO:_FillValue = -999.f ;
float SEA_ICE_CONCENTRATION_at_ARGO(N_prof) ;
SEA_ICE_CONCENTRATION_at_ARGO:long_name = "Daily sea ice area fraction (EUMETSAT OSI-SAF OSI-450) at Argo float location (%)" ;
SEA_ICE_CONCENTRATION_at_ARGO:units = "1" ;
SEA_ICE_CONCENTRATION_at_ARGO:standard_name = "sea_ice_area_fraction" ;
SEA_ICE_CONCENTRATION_at_ARGO:_FillValue = -999.f ;
float CCMP_6h_Wind_Speed_at_ARGO(N_prof) ;
CCMP_6h_Wind_Speed_at_ARGO:long_name = "6-hourly CCMP wind speed at Argo float

location" ;
CCMP_6h_Wind_Speed_at_ARGO:units = "m s-1" ;
CCMP_6h_Wind_Speed_at_ARGO:standard_name = "wind_speed" ;
CCMP_6h_Wind_Speed_at_ARGO:_FillValue = -999.f ;
float CCMP_10_prior_days_Wind_Speed_at_ARGO(N_prof, N_DAYS_WIND_CCMP) ;
CCMP_10_prior_days_Wind_Speed_at_ARGO:long_name = "Prior 10 days time series of CCMP wind speed at Argo float location" ;
CCMP_10_prior_days_Wind_Speed_at_ARGO:units = "m s-1" ;
CCMP_10_prior_days_Wind_Speed_at_ARGO:standard_name = "wind_speed" ;
CCMP_10_prior_days_Wind_Speed_at_ARGO:_FillValue = -999.f ;
float CDM_GLOBCOLOUR_at_ARGO(N_prof) ;
CDM_GLOBCOLOUR_at_ARGO:long_name = "8-day Coloured dissolved and detrital organic materials - mean of the binned pixels at Argo float location" ;
CDM_GLOBCOLOUR_at_ARGO:units = "m-1" ;
CDM_GLOBCOLOUR_at_ARGO:standard_name = "volume_absorption_coefficient_of_radiative_flux_in_sea_wate
;
CDM_GLOBCOLOUR_at_ARGO:_FillValue = -999.f ;
float CHL1_GLOBCOLOUR_at_ARGO(N_prof) ;
CHL1_GLOBCOLOUR_at_ARGO:long_name = "8-day Chlorophyll concentration - mean of the binned pixels at Argo float location" ;
CHL1_GLOBCOLOUR_at_ARGO:units = "mg m-3" ;
CHL1_GLOBCOLOUR_at_ARGO:standard_name = "mass_concentration_of_chlorophyll_a_in_sea_water"
;
CHL1_GLOBCOLOUR_at_ARGO:_FillValue = -999.f ;
float EVAPORATION_OAFLUX_at_ARGO(N_prof) ;
EVAPORATION_OAFLUX_at_ARGO:long_name = "Daily mean evaporation rate (OAFlux) at Argo float location" ;
EVAPORATION_OAFLUX_at_ARGO:units = "cm year-1" ;
EVAPORATION_OAFLUX_at_ARGO:_FillValue = -999.f ;
float SSS_SCRIPPS_at_ARGO(N_prof) ;
SSS_SCRIPPS_at_ARGO:long_name = "Argo gridded monthly mean SSS (0m depth) from SCRIPPS (Roemmich-Gilson) at Argo float location" ;
SSS_SCRIPPS_at_ARGO:units = "1" ;
SSS_SCRIPPS_at_ARGO:salinity_scale = "Practical Salinity Scale (PSS-78)" ;
SSS_SCRIPPS_at_ARGO:standard_name = "sea_water_salinity" ;
SSS_SCRIPPS_at_ARGO:_FillValue = -999.f ;
float SSS_IPRC_at_ARGO(N_prof) ;
SSS_IPRC_at_ARGO:long_name = "Argo gridded monthly mean SSS (0m depth) from IPRC at Argo float location" ;
SSS_IPRC_at_ARGO:units = "1" ;
SSS_IPRC_at_ARGO:salinity_scale = "Practical Salinity Scale (PSS-78)" ;
SSS_IPRC_at_ARGO:standard_name = "sea_water_salinity" ;
SSS_IPRC_at_ARGO:_FillValue = -999.f ;
float SST_AVHRR_at_ARGO(N_prof) ;
SST_AVHRR_at_ARGO:long_name = "Daily OI AVHRR-only v2 SST (Reynolds et al., 2007) at Argo float location" ;
SST_AVHRR_at_ARGO:units = "degree Celsius" ;
SST_AVHRR_at_ARGO:standard_name = "sea_water_temperature" ;
SST_AVHRR_at_ARGO:_FillValue = -999.f ;

float U_EKMAN_GLOBCURRENT_at_ARGO(N_prof) ;
U_EKMAN_GLOBCURRENT_at_ARGO:long_name = "15m depth Ekman current velocity: zonal component at Argo float location" ;
U_EKMAN_GLOBCURRENT_at_ARGO:units = "m s-1" ;
U_EKMAN_GLOBCURRENT_at_ARGO:_FillValue = -999.f ;
float V_EKMAN_GLOBCURRENT_at_ARGO(N_prof) ;
V_EKMAN_GLOBCURRENT_at_ARGO:long_name = "15m depth Ekman current velocity: meridian component at Argo float location" ;
V_EKMAN_GLOBCURRENT_at_ARGO:units = "m s-1" ;
V_EKMAN_GLOBCURRENT_at_ARGO:_FillValue = -999.f ;
float U_GEOSTROPHIC_GLOBCURRENT_at_ARGO(N_prof) ;
U_GEOSTROPHIC_GLOBCURRENT_at_ARGO:long_name = "Absolute geostrophic velocity: zonal component at Argo float location" ;
U_GEOSTROPHIC_GLOBCURRENT_at_ARGO:units = "m s-1" ;
U_GEOSTROPHIC_GLOBCURRENT_at_ARGO:_FillValue = -999.f ;
float V_GEOSTROPHIC_GLOBCURRENT_at_ARGO(N_prof) ;
V_GEOSTROPHIC_GLOBCURRENT_at_ARGO:long_name = "Absolute geostrophic velocity: meridian component at Argo float location" ;
V_GEOSTROPHIC_GLOBCURRENT_at_ARGO:units = "m s-1" ;
V_GEOSTROPHIC_GLOBCURRENT_at_ARGO:_FillValue = -999.f ;

// global attributes:
:Conventions = "CF-1.6" ;
:title = "ARGO Match-Up Database" ;
:Satellite_product_name = "SMOS-L2-DPGS-v662" ;
:Satellite_product_spatial_resolution = "30 km" ;
:Satellite_product_temporal_resolution = "50 min" ;
:Satellite_product_filename = "netcdf/2010/06/01/SM_REPR_MIR_OSUDP2_20100601T000131_20100601T001849_662_120_1.nc" ;
:Match-Up_spatial_window_radius_in_km = 25;
:Match-Up_temporal_window_radius_in_days = 0.5;
:start_time = "20100114T000005Z" ;
:stop_time = "20100118T235026Z" ;
:northernmost_latitude = 77.676f ;
:sourthenmost_latitude = -66.423f ;
:westernmost_longitude = -179.219f ;
:easternmost_longitude = 179.199f ;
:geospatial_lat_units = "degrees north" ;
:geospatial_lat_resolution = "30 km" ;
:geospatial_lon_units = "degrees east" ;
:geospatial_lon_resolution = "30 km" ;
:institution = "ESA-IFREMER-ODL-OCEANSCOPE" ;
:project_name = "SMOS Pilot-Mission Exploitation Platform (Pi-MEP) for salinity" ;
:project_url = "https://www.salinity-pimep.org" ;
:license = "Pi-MEP data use is free and open" ;
:product_version = "1.0" ;
:keywords = "Oceans > Ocean Salinity > Sea Surface Salinity" ;
:acknowledgment = "Please acknowledge the use of these data with the following statement: These data were provided by the SMOS Pilot-Mission Exploitation Platform (Pi-MEP)

for salinity" ;
:source = "netcdf/2010/06/01/SM_REPR_MIR_OSUDP2_20100601T000131_20100601T001849_662_120_1.nc" ;
:In_situ_data_source = "ftp://ftp.ifremer.fr/ifremer/argo/geo/" ;
:references = "https://www.salinity-pimep.org" ;
:history = "Processed on 2018-04-18 using MDB_generator" ;
:date_created = "2018-04-18 17:09:30" ;
}

2.5 MDB characteristics for the particular *in situ*/satellite pairs

2.5.1 Number of paired SSS data as a function of time and distance to coast

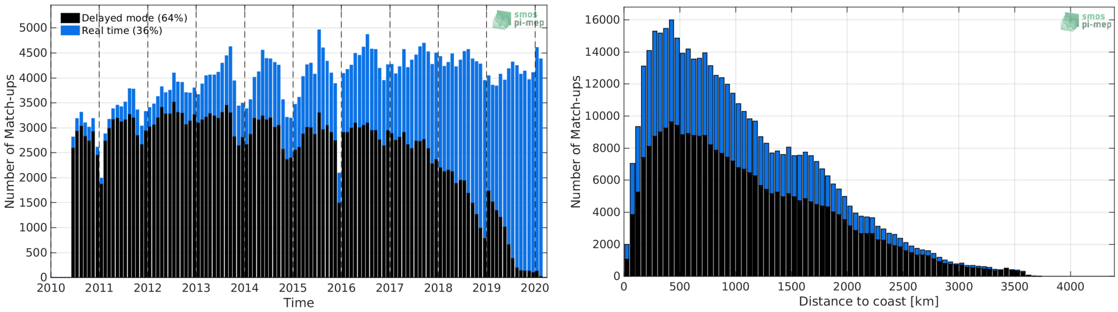

(a) (b)

Figure 1: Number of match-ups between Argo and SMOS-L2-DPGS-v662 SSS as a function of time (a) and as function of the distance to coast (b) over the Global Ocean Pi-MEP region and for the full satellite product period.

2.5.2 Histograms of the SSS match-ups

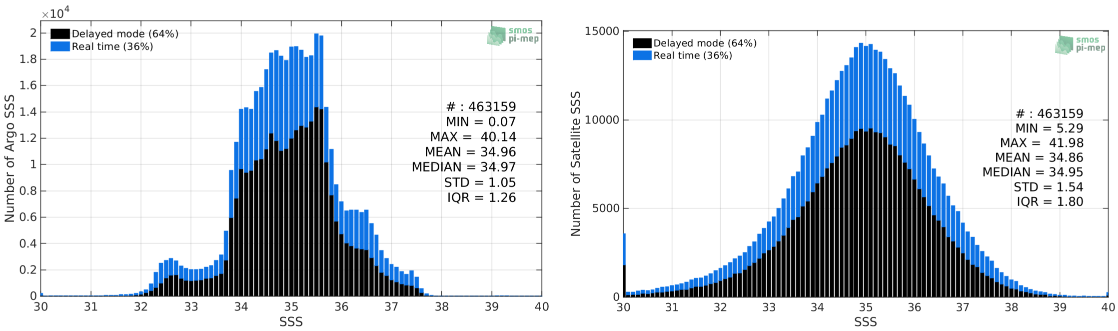

(a) (b)

Figure 2: Histograms of SSS from Argo (a) and SMOS-L2-DPGS-v662 (b) considering all match-up pairs per bins of 0.1 over the Global Ocean Pi-MEP region and for the full satellite product period.

2.5.3 Distribution of *in situ* SSS depth measurements

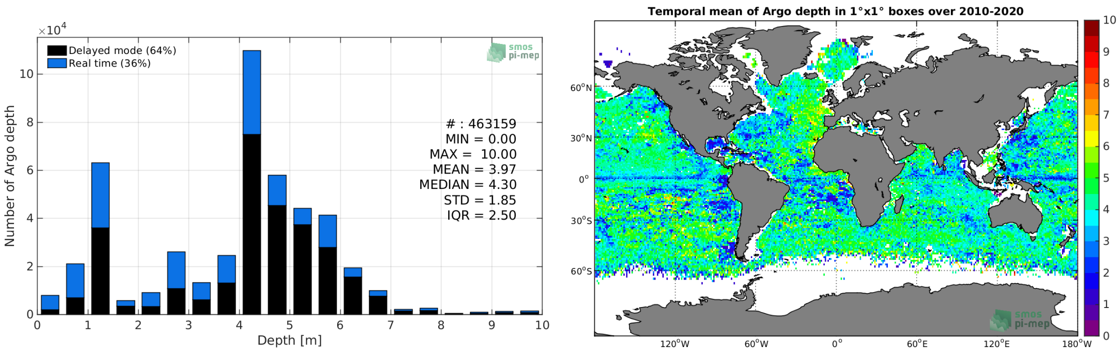

(a) (b)

Figure 3: Histograms of the depth of the upper level SSS measurements from Argo in the Match-up DataBase for the Global Ocean Pi-MEP region (a) and temporal mean spatial distribution of pressure of the *in situ* SSS data over 1°x1° boxes and for the full satellite product period (b).

2.5.4 Spatial Distribution of Match-ups

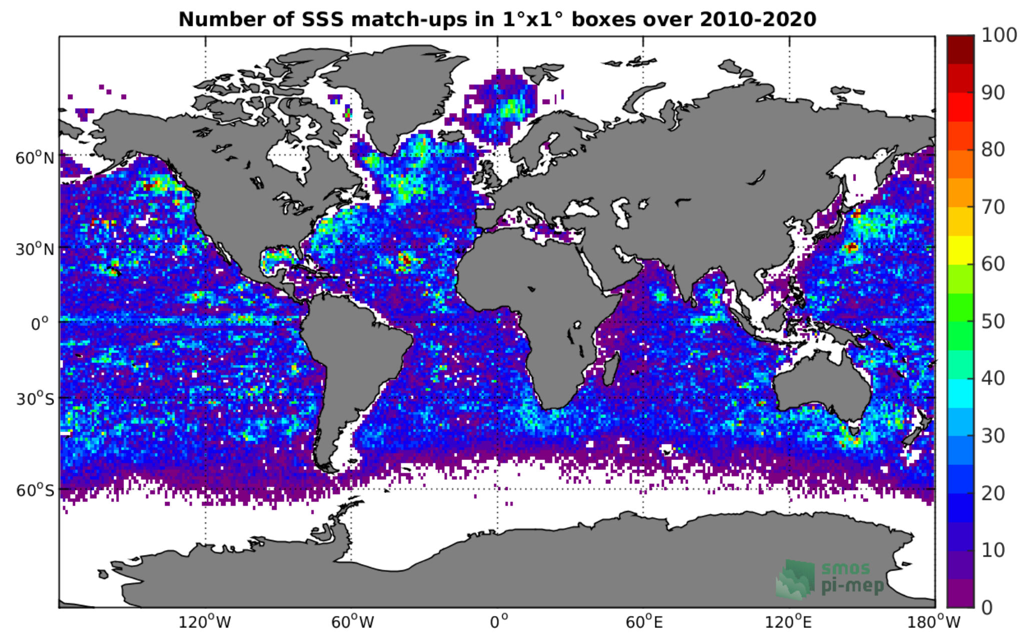

Figure 4: Number of SSS match-ups between Argo SSS and the SMOS-L2-DPGS-v662 SSS product for the Global Ocean Pi-MEP region over 1°x1° boxes and for the full satellite product period.

2.5.5 Histograms of the spatial and temporal lags of the match-ups pairs

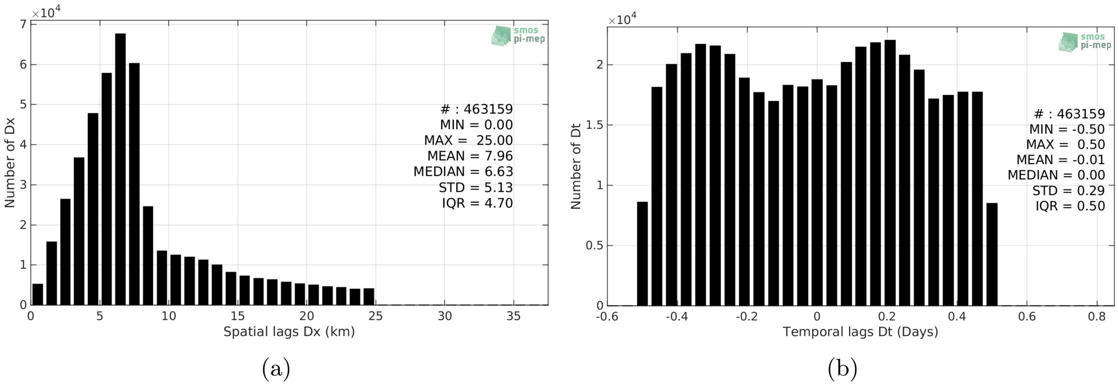

Figure 5: Histograms of the spatial (a) and temporal (b) lags between the time of the Argo measurements and the date of the corresponding SMOS-L2-DPGS-v662 SSS product.

3 MDB file Analyses

3.1 Spatial Maps of the Temporal mean and Std of *in situ* and satellite SSS and of the difference (ΔSSS)

3.1.1 Ascending and Descending orbits

In Figure 6, we show maps of temporal mean (left) and standard deviation (right) of the SMOS-L2-DPGS-v662 (top) and of the Argo *in situ* dataset at the collected Pi-MEP match-up pairs. The temporal mean and std are gridded over the full satellite product period and over spatial boxes of size 1°x1°.

At the bottom of Figure 6, the temporal mean (left) and standard deviation (right) of the differences between the satellite SSS product and *in situ* data found at match-up pairs, namely ΔSSS(Satellite -Argo), is also gridded over the full satellite product period and over spatial boxes of size 1°x1°.

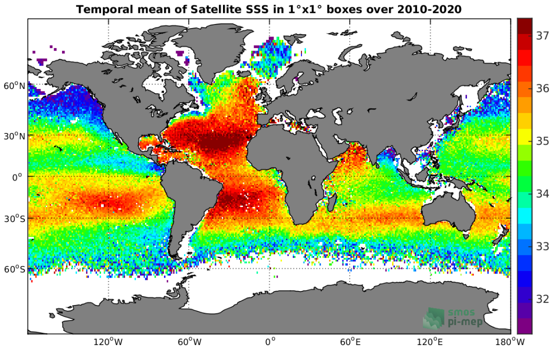

(a) MEAN(Satellite SSS)

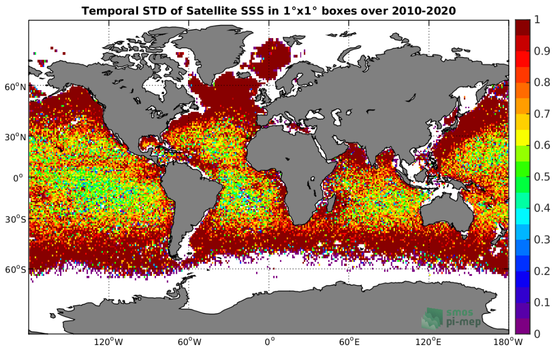

(b) Std(Satellite SSS)

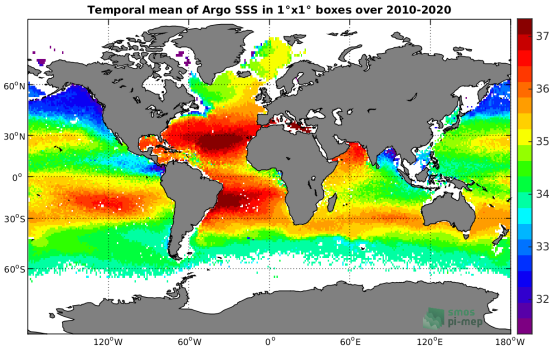

(c) MEAN(Argo SSS)

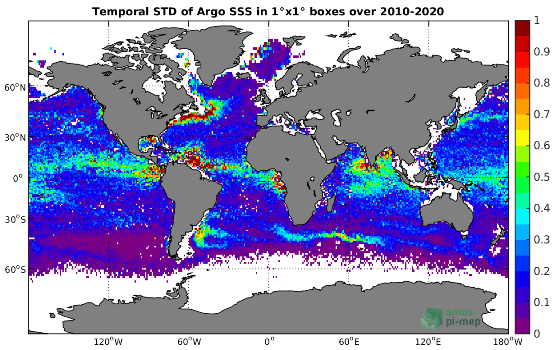

(d) Std(Argo SSS)

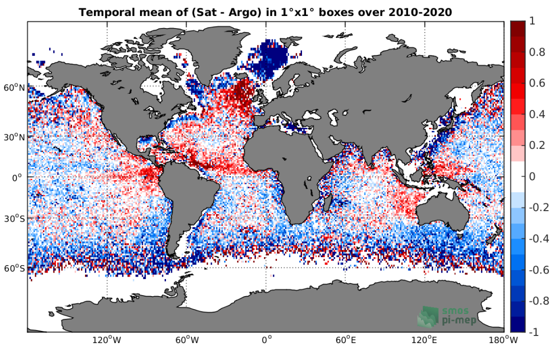

(e) MEAN(ΔSSS) (Satellite - Argo)

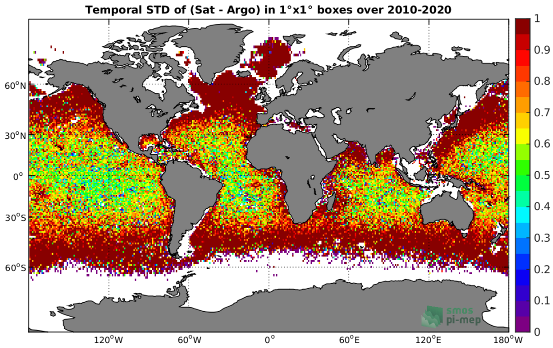

(f) Std(ΔSSS) (Satellite - Argo)

Figure 6: Temporal mean (left) and Std (right) of SSS from SMOS-L2-DPGS-v662 (top), Argo (middle), and of ΔSSS (Satellite - Argo). Only match-up pairs are used to generate these maps.

3.1.2 Ascending orbits

In Figure 7, we show maps of temporal mean (left) and standard deviation (right) of the SMOS-L2-DPGS-v662 (top) and of the Argo *in situ* dataset at the collected Pi-MEP match-up pairs. The temporal mean and std are gridded over the full satellite product period and over spatial boxes of size 1°x1°.

At the bottom of Figure 7, the temporal mean (left) and standard deviation (right) of the differences between the satellite SSS product and *in situ* data found at match-up pairs, namely ΔSSS(Satellite -Argo), is also gridded over the full satellite product period and over spatial boxes of size 1°x1°.

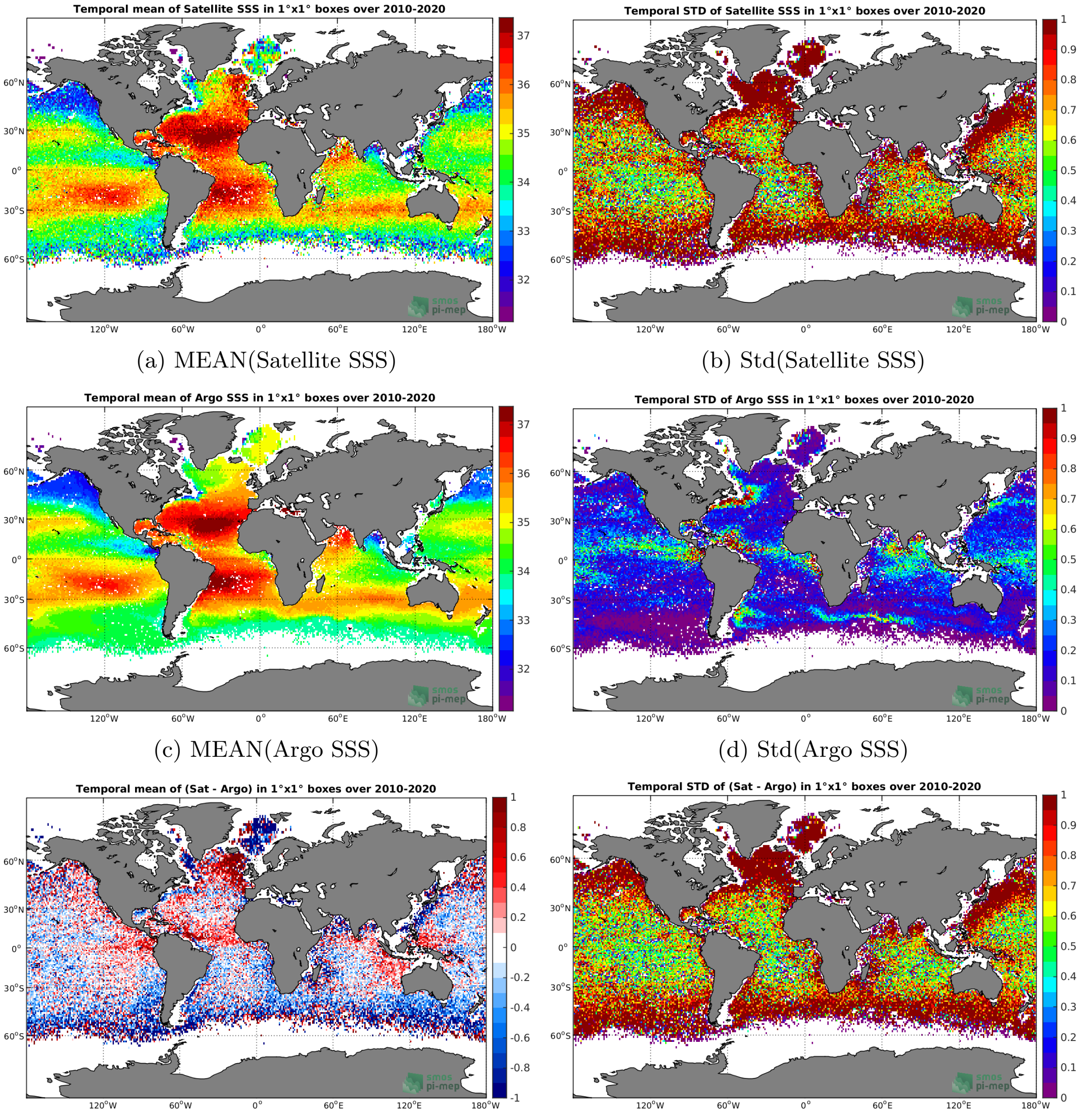

(a) MEAN(Satellite SSS) (b) Std(Satellite SSS)

(c) MEAN(Argo SSS) (d) Std(Argo SSS)

(e) MEAN(ΔSSS) (Satellite - Argo) (f) Std(ΔSSS) (Satellite - Argo)

Figure 7: Temporal mean (left) and Std (right) of SSS from SMOS-L2-DPGS-v662 (top), Argo (middle), and of ΔSSS (Satellite - Argo). Only match-up pairs and ascending orbits are used to generate these maps.

3.1.3 Descending orbits

In Figure 8, we show maps of temporal mean (left) and standard deviation (right) of the SMOS-L2-DPGS-v662 (top) and of the Argo *in situ* dataset at the collected Pi-MEP match-up pairs. The temporal mean and std are gridded over the full satellite product period and over spatial boxes of size 1°x1°.

At the bottom of Figure 8, the temporal mean (left) and standard deviation (right) of the differences between the satellite SSS product and *in situ* data found at match-up pairs, namely ΔSSS(Satellite -Argo), is also gridded over the full satellite product period and over spatial boxes of size 1°x1°.

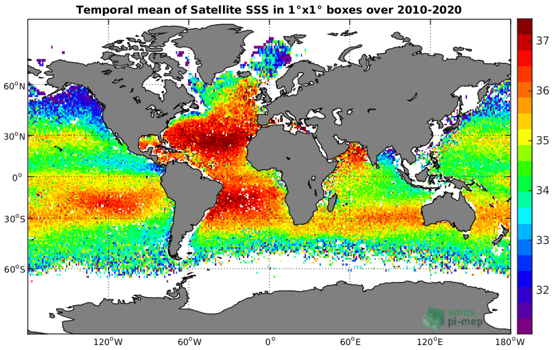

(a) MEAN(Satellite SSS)

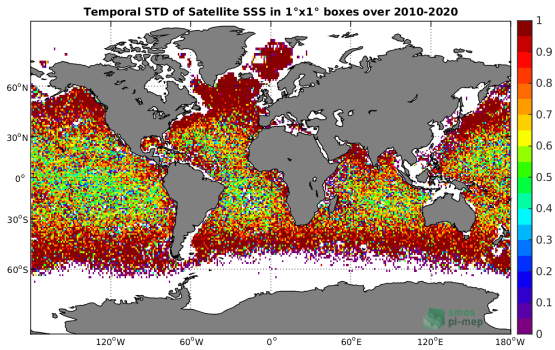

(b) Std(Satellite SSS)

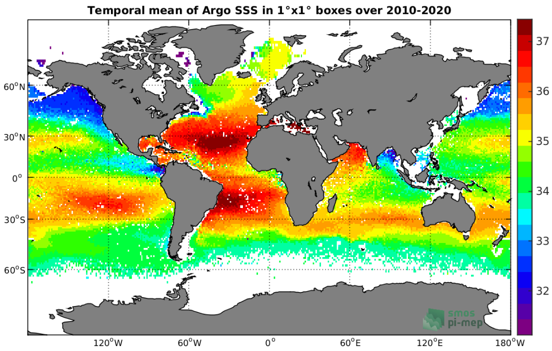

(c) MEAN(Argo SSS)

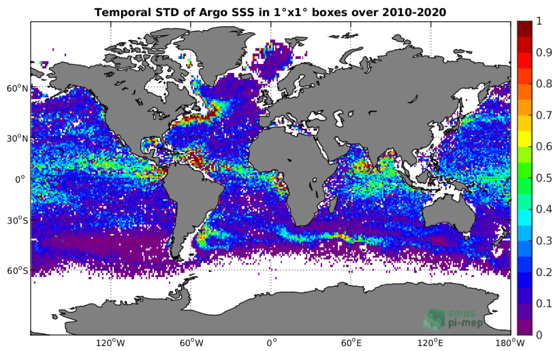

(d) Std(Argo SSS)

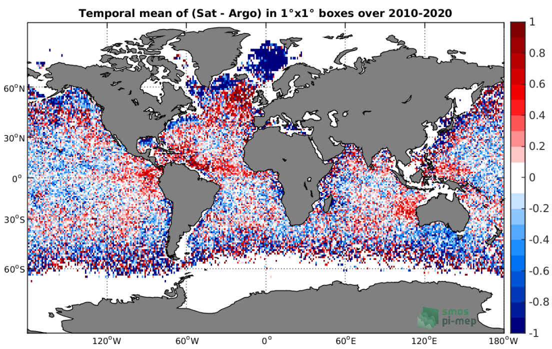

(e) MEAN(ΔSSS) (Satellite - Argo)

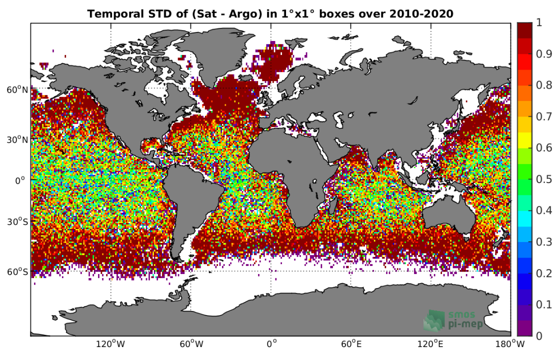

(f) Std(ΔSSS) (Satellite - Argo)

Figure 8: Temporal mean (left) and Std (right) of SSS from SMOS-L2-DPGS-v662 (top), Argo (middle), and of ΔSSS (Satellite - Argo). Only match-up pairs and descending orbits are used to generate these maps.

3.2 Time series of the monthly median and Std of *in situ* and satellite SSS and of the (ΔSSS)

3.2.1 Ascending and Descending orbits

In the top panel of Figure 9, we show the time series of the monthly median SSS estimated over the full Global Ocean Pi-MEP region for both SMOS-L2-DPGS-v662 satellite SSS product (in black) and the Argo *in situ* dataset (in blue) at the collected Pi-MEP match-up pairs.

In the middle panel of Figure 9, we show the time series of the monthly median of ΔSSS (Satellite - Argo) for the collected Pi-MEP match-up pairs and estimated over the full Global Ocean Pi-MEP region.

In the bottom panel of Figure 9, we show the time series of the monthly standard deviation of the ΔSSS (Satellite - Argo) for the collected Pi-MEP match-up pairs and estimated over the full Global Ocean Pi-MEP region.

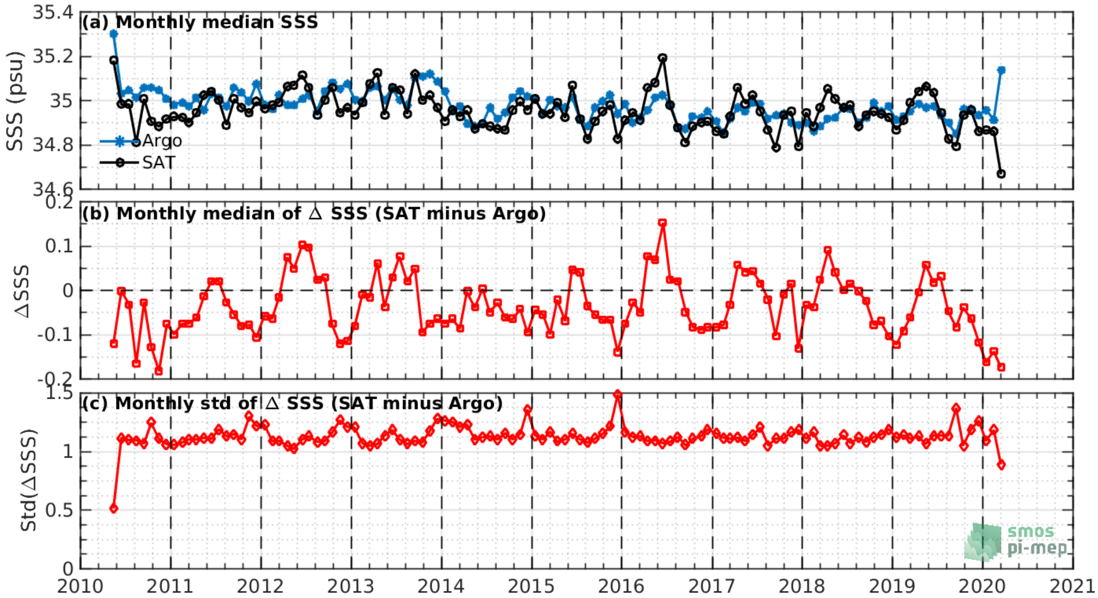

Figure 9: Time series of the monthly median SSS (top), median of ΔSSS (Satellite - Argo) and Std of ΔSSS (Satellite - Argo) over the Global Ocean Pi-MEP region considering all match-ups collected by the Pi-MEP.

3.2.2 Ascending orbits

In the top panel of Figure 10, we show the time series of the monthly median SSS estimated over the full Global Ocean Pi-MEP region for both SMOS-L2-DPGS-v662 satellite SSS product (in black) and the Argo *in situ* dataset (in blue) at the collected Pi-MEP match-up pairs.

In the middle panel of Figure 10, we show the time series of the monthly median of ΔSSS (Satellite - Argo) for the collected Pi-MEP match-up pairs and estimated over the full Global Ocean Pi-MEP region.

In the bottom panel of Figure 10, we show the time series of the monthly standard deviation of the ΔSSS (Satellite - Argo) for the collected Pi-MEP match-up pairs and estimated over the full Global Ocean Pi-MEP region.

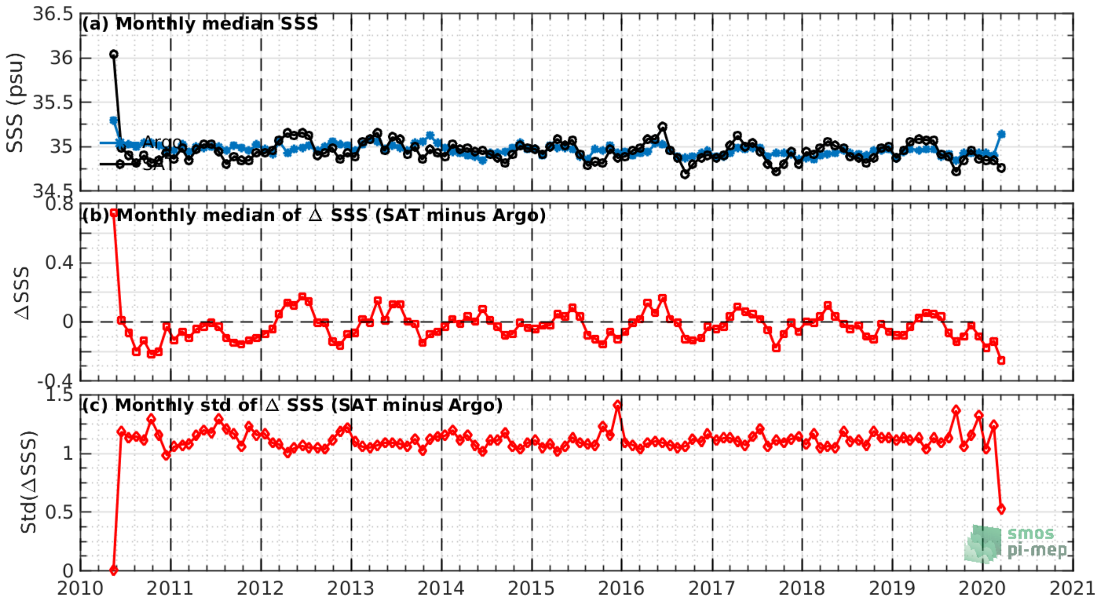

Figure 10: Time series of the monthly median SSS (top), median of ΔSSS (Satellite - Argo) and Std of ΔSSS (Satellite - Argo) over the Global Ocean Pi-MEP region considering only ascending orbits from all match-ups collected by the Pi-MEP.

3.2.3 Descending orbits

In the top panel of Figure 11, we show the time series of the monthly median SSS estimated over the full Global Ocean Pi-MEP region for both SMOS-L2-DPGS-v662 satellite SSS product (in black) and the Argo *in situ* dataset (in blue) at the collected Pi-MEP match-up pairs.

In the middle panel of Figure 11, we show the time series of the monthly median of ΔSSS (Satellite - Argo) for the collected Pi-MEP match-up pairs and estimated over the full Global Ocean Pi-MEP region.

In the bottom panel of Figure 11, we show the time series of the monthly standard deviation of the ΔSSS (Satellite - Argo) for the collected Pi-MEP match-up pairs and estimated over the full Global Ocean Pi-MEP region.

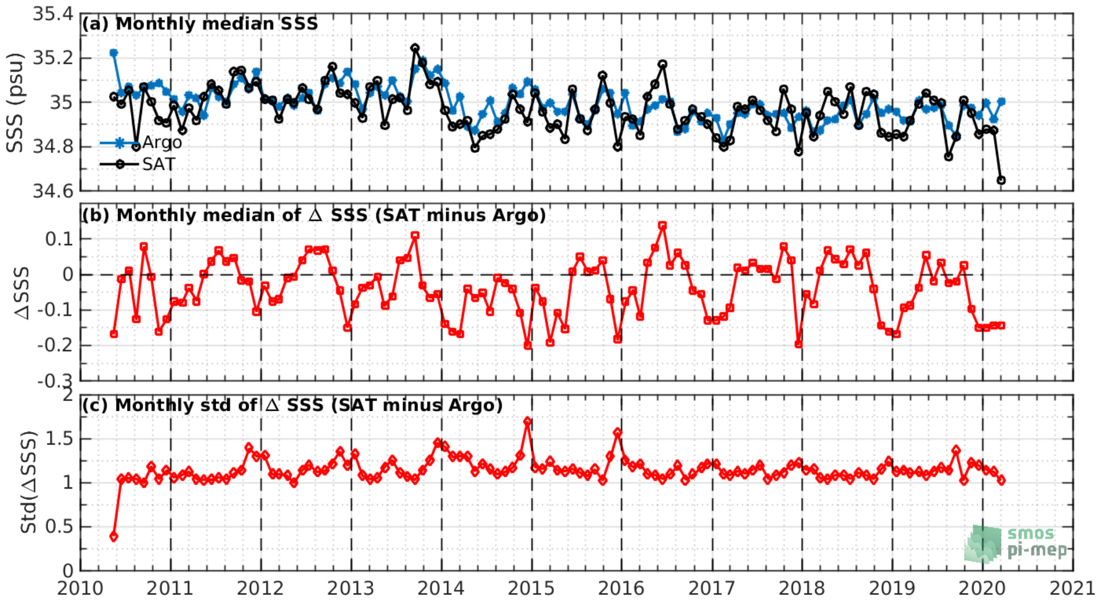

Figure 11: Time series of the monthly median SSS (top), median of ΔSSS (Satellite - Argo) and Std of ΔSSS (Satellite - Argo) over the Global Ocean Pi-MEP region considering only descending orbits from all match-ups collected by the Pi-MEP.

3.3 Zonal mean and Std of *in situ* and satellite SSS and of the ΔSSS

3.3.1 Ascending and Descending orbits

In Figure 12 left panel, we show the zonal mean SSS considering all Pi-MEP match-up pairs for both SMOS-L2-DPGS-v662 satellite SSS product (in black) and the Argo *in situ* dataset (in blue). Solid lines and dashed lines correspond to the use of the full satellite SSS product period and the last month of data, respectively, to derive the mean.

In the right panel of Figure 12, we show the zonal mean of ΔSSS (Satellite - Argo) for all the collected Pi-MEP match-up pairs estimated over the full satellite product period (solid line) and the last month of data (dashed line).

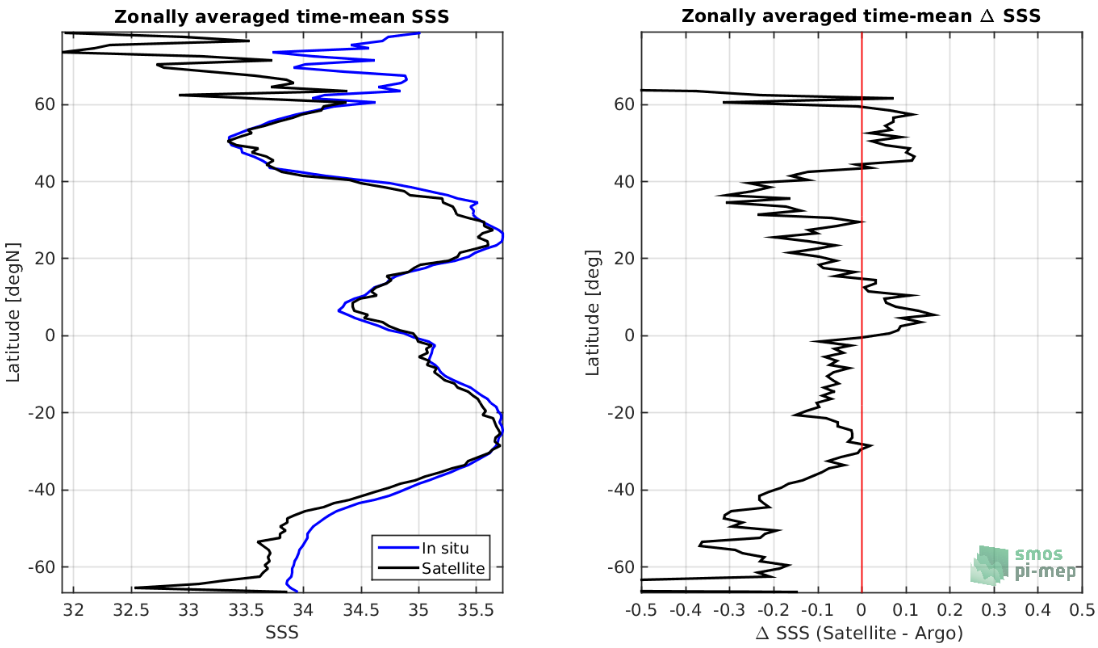

Figure 12: Left panel: Zonal mean SSS from SMOS-L2-DPGS-v662 (black) and from Argo (blue). Right panel: Zonal mean of ΔSSS (Satellite - Argo) for all the collected Pi-MEP match-up pairs estimated over the full satellite product period.

3.3.2 Ascending orbits

In Figure 13 left panel, we show the zonal mean SSS considering only ascending orbits from all Pi-MEP match-up pairs for both SMOS-L2-DPGS-v662 satellite SSS product (in black) and the Argo *in situ* dataset (in blue). Solid lines and dashed lines correspond to the use of the full satellite SSS product period and the last month of data, respectively, to derive the mean.

In the right panel of Figure 13, we show the zonal mean of ΔSSS (Satellite - Argo) considering only ascending orbits from all the collected Pi-MEP match-up pairs estimated over the full satellite product period (solid line) and the last month of data (dashed line).

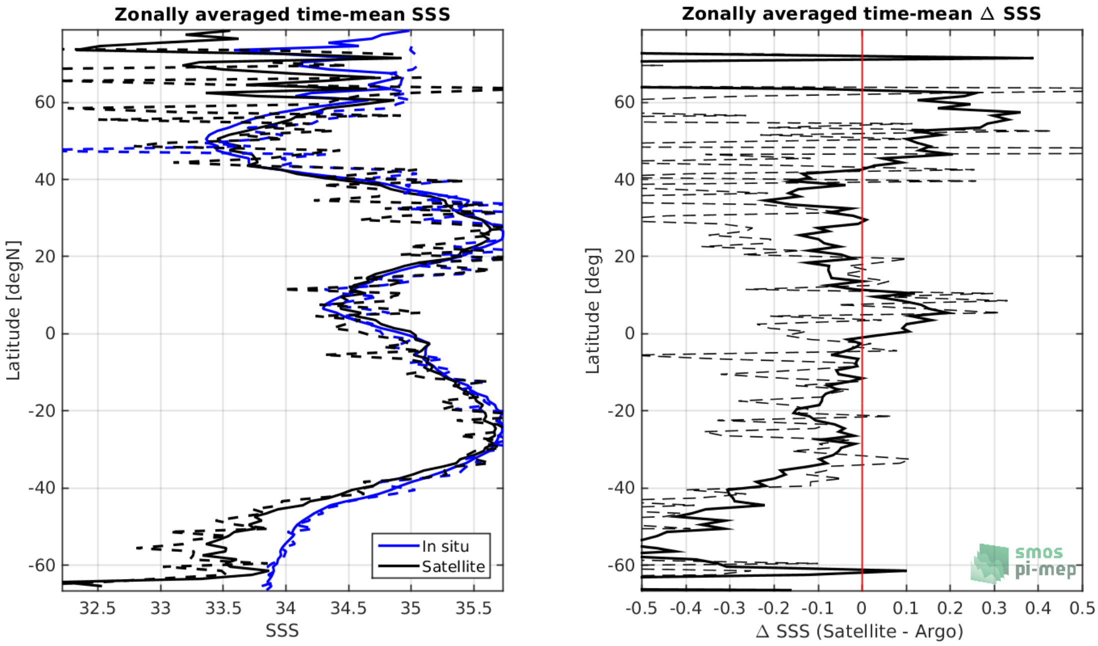

Figure 13: Left panel: Zonal mean SSS from SMOS-L2-DPGS-v662 satellite product (black) and from Argo (blue). Right panel: Zonal mean of ΔSSS (Satellite - Argo) considering only ascending orbits from all the collected Pi-MEP match-up pairs estimated over the full satellite product period. The dash curves correspond to the same estimates but considering only the last month of data.

3.3.3 Decending orbits

In Figure 14 left panel, we show the zonal mean SSS considering only descending orbits from all Pi-MEP match-up pairs for both SMOS-L2-DPGS-v662 satellite SSS product (in black) and the Argo *in situ* dataset (in blue). Solid lines and dashed lines correspond to the use of the full satellite SSS product period and the last month of data, respectively, to derive the mean.

In the right panel of Figure 14, we show the zonal mean of ΔSSS (Satellite - Argo) considering only descending orbits from all the collected Pi-MEP match-up pairs estimated over the full satellite product period (solid line) and the last month of data (dashed line).

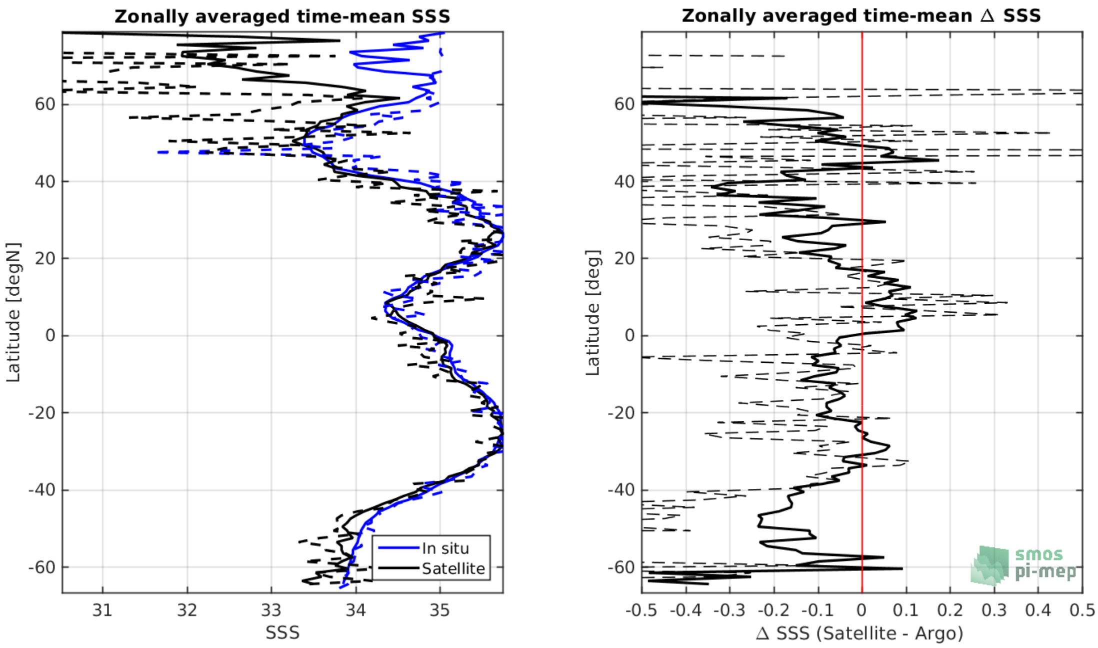

Figure 14: Left panel: Zonal mean SSS from SMOS-L2-DPGS-v662 satellite product (black) and from Argo (blue). Right panel: Zonal mean of ΔSSS (Satellite - Argo) considering only descending orbits from all the collected Pi-MEP match-up pairs estimated over the full satellite product period. The dash curves correspond to the same estimates but considering only the last month of data.

3.4 Scatterplots of satellite vs *in situ* SSS by latitudinal bands

For Figures 15, 16 and 17, we use only the last month of match-up pairs.

3.4.1 Ascending and Descending orbits

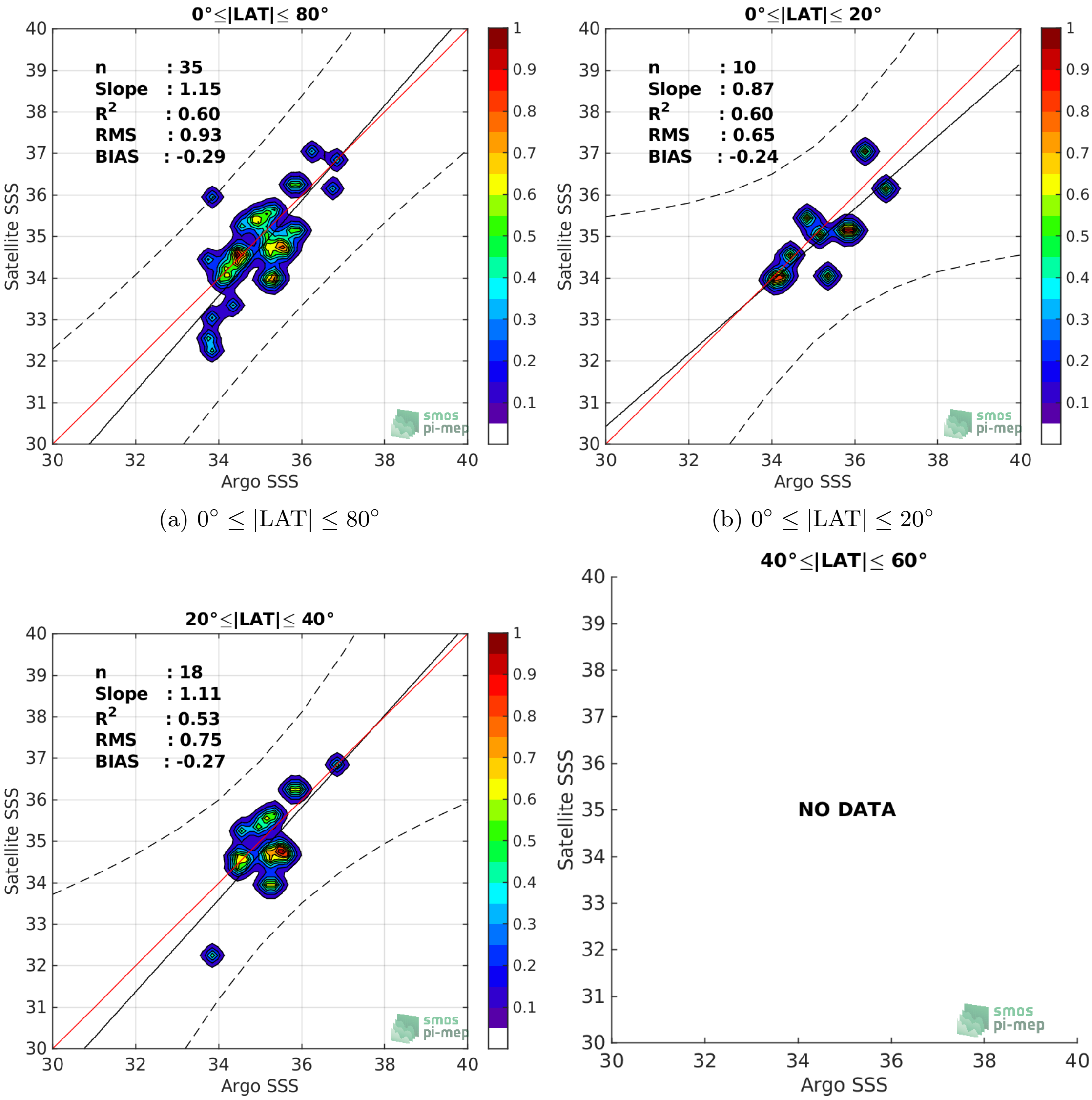

(a) $0° \leq |\text{LAT}| \leq 80°$ (b) $0° \leq |\text{LAT}| \leq 20°$

(c) $20° \leq |\text{LAT}| \leq 40°$ (d) $40° \leq |\text{LAT}| \leq 60°$

Figure 15: Contour maps of the concentration of SMOS-L2-DPGS-v662 SSS (y-axis) versus Argo SSS (x-axis) at match-up pairs for different latitude bands. For each plot, the red line shows x=y. The black thin and dashed lines indicate a linear fit through the data cloud and the ±95% confidence levels, respectively. The number match-up pairs n, the slope and R^2 coefficient of the linear fit, the root mean square (RMS) and the mean bias between satellite and *in situ* data are indicated for each latitude band in each plots.

3.4.2 Ascending orbits

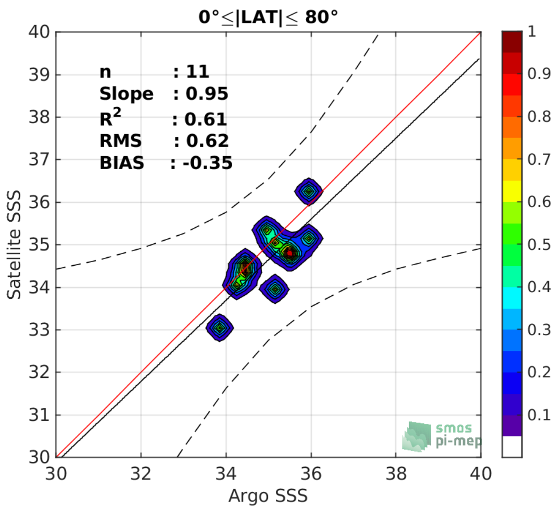

(a) 0° ≤ |LAT| ≤ 80°

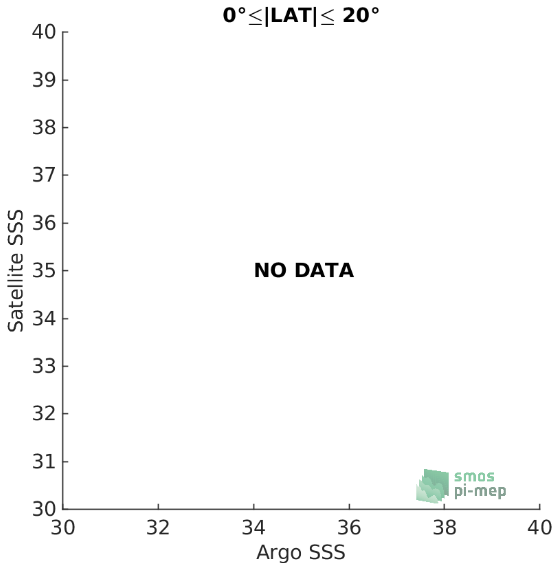

(b) 0° ≤ |LAT| ≤ 20°

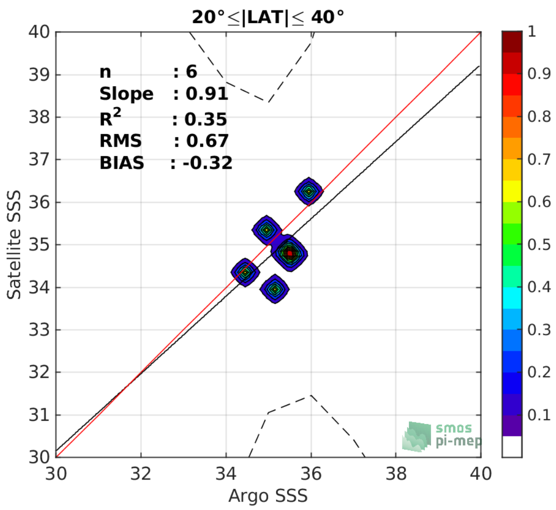

(c) 20° ≤ |LAT| ≤ 40°

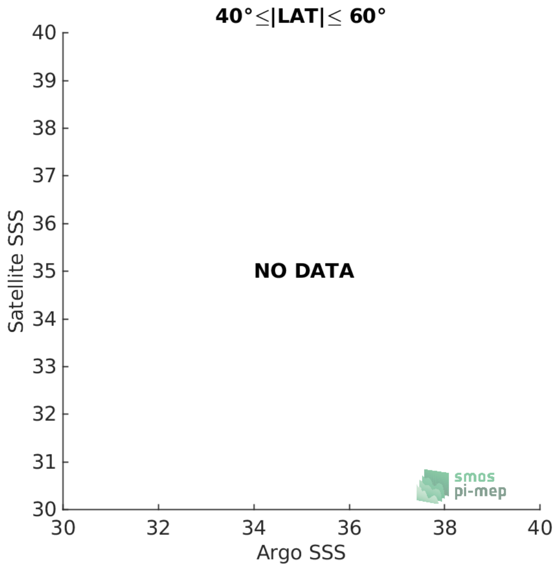

(d) 40° ≤ |LAT| ≤ 60°

Figure 16: Contour maps of the concentration of SMOS-L2-DPGS-v662 SSS (y-axis) versus Argo SSS (x-axis) at match-up pairs for different latitude bands. For each plot, the red line shows x=y. The black thin and dashed lines indicate a linear fit through the data cloud and the ±95% confidence levels, respectively. The number match-up pairs n, the slope and R^2 coefficient of the linear fit, the root mean square (RMS) and the mean bias between satellite and *in situ* data are indicated for each latitude band in each plots.

3.4.3 Descending orbits

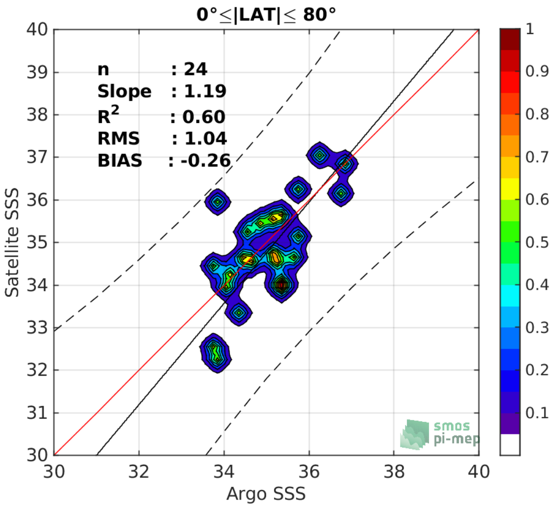

(a) 0° ≤ |LAT| ≤ 80°

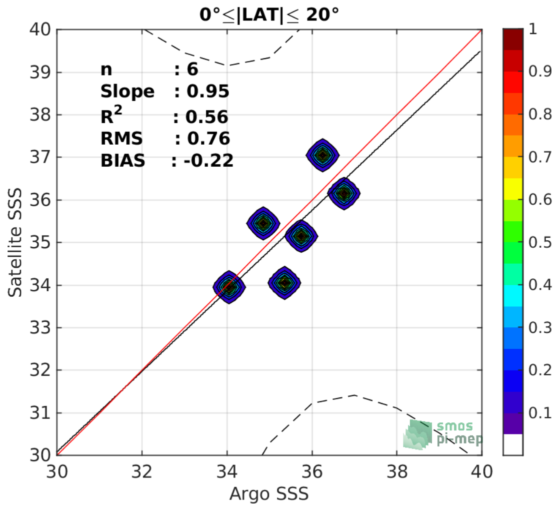

(b) 0° ≤ |LAT| ≤ 20°

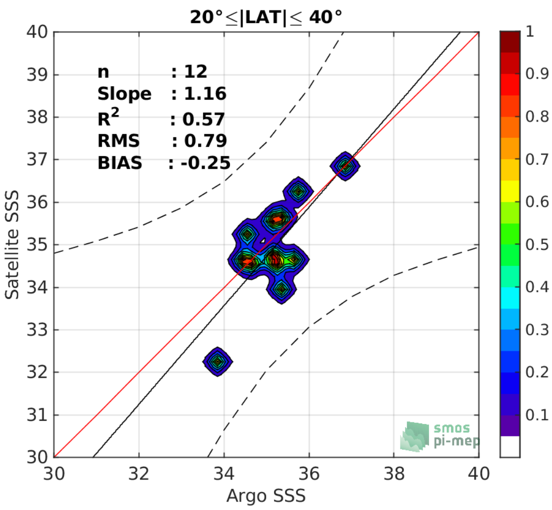

(c) 20° ≤ |LAT| ≤ 40°

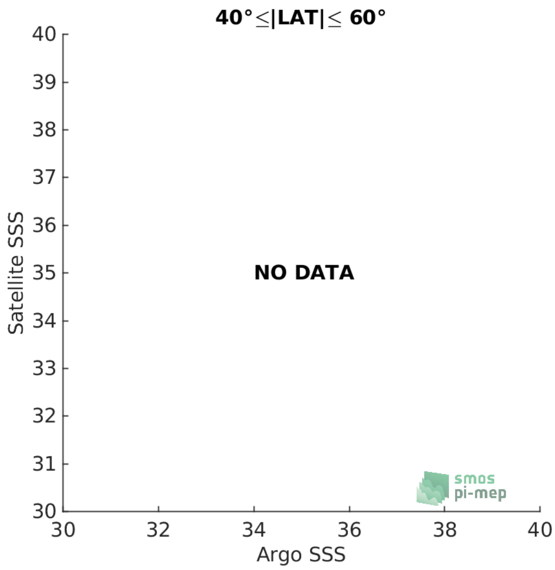

(d) 40° ≤ |LAT| ≤ 60°

Figure 17: Contour maps of the concentration of SMOS-L2-DPGS-v662 SSS (y-axis) versus Argo SSS (x-axis) at match-up pairs for different latitude bands. For each plot, the red line shows x=y. The black thin and dashed lines indicate a linear fit through the data cloud and the ±95% confidence levels, respectively. The number match-up pairs n, the slope and R^2 coefficient of the linear fit, the root mean square (RMS) and the mean bias between satellite and *in situ* data are indicated for each latitude band in each plots.

3.5 Time series of the monthly median and Std of the ΔSSS sorted by latitudinal bands

3.5.1 Ascending and Descending orbits

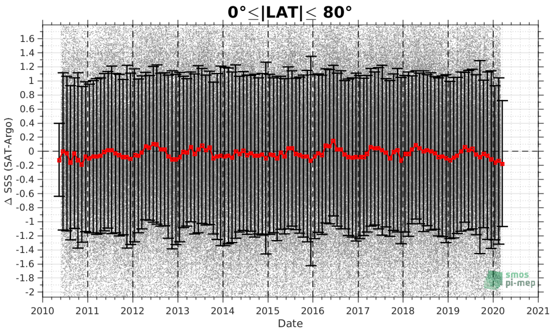

(a) 0° ≤ |LAT| ≤ 80°

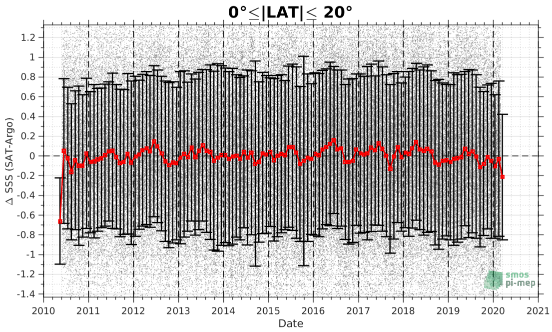

(b) 0° ≤ |LAT| ≤ 20°

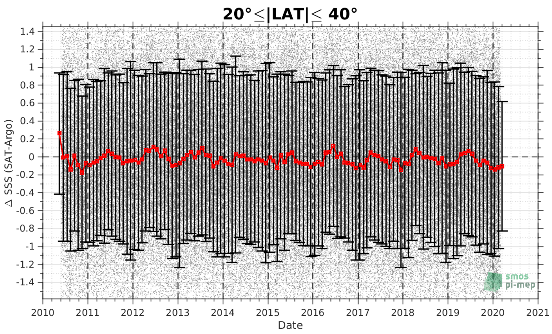

(c) 20° ≤ |LAT| ≤ 40°

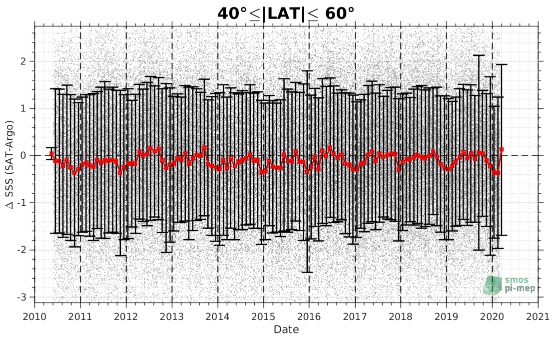

(d) 40° ≤ |LAT| ≤ 60°

Figure 18: Monthly median (red curves) of ΔSSS (Satellite - Argo) and ±1 Std (black vertical thick bars) as function of time for all the collected Pi-MEP match-up pairs estimated over the Global Ocean Pi-MEP region and for the full satellite product period are shown for different latitude bands: (a) 80°S-80°N, (b) 20°S-20°N, (c) 40°S-20°S and 20°N-40°N and (d) 60°S-40°S and 40°N-60°N.

3.5.2 Ascending orbits

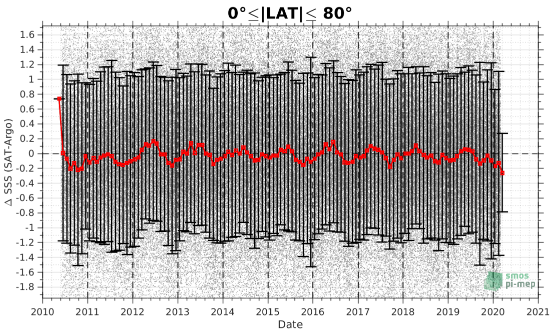

(a) 0° ≤ |LAT| ≤ 80°

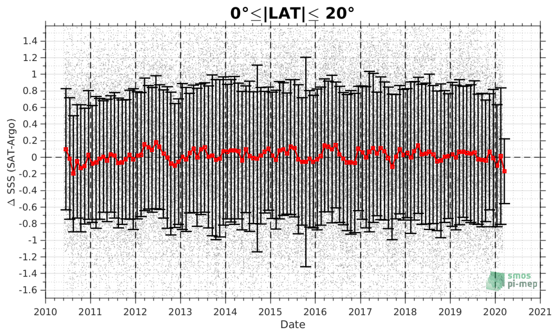

(b) 0° ≤ |LAT| ≤ 20°

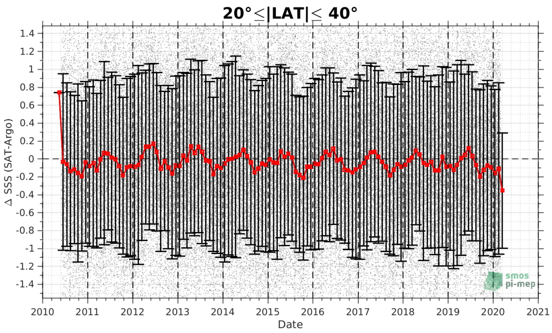

(c) 20° ≤ |LAT| ≤ 40°

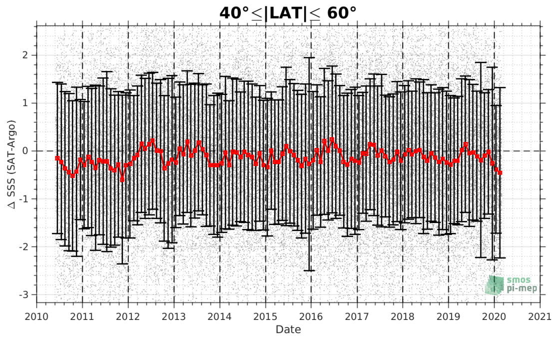

(d) 40° ≤ |LAT| ≤ 60°

Figure 19: Monthly median (red curves) of ΔSSS (Satellite - Argo) and ±1 Std (black vertical thick bars) as function of time for all the collected Pi-MEP match-up pairs estimated over the Global Ocean Pi-MEP region and for the full satellite product period are shown for different latitude bands: (a) 80°S-80°N, (b) 20°S-20°N, (c) 40°S-20°S and 20°N-40°N and (d) 60°S-40°S and 40°N-60°N.

3.5.3 Descending orbits

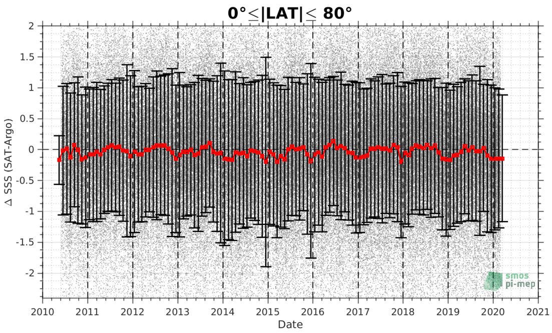

(a) 0° ≤ |LAT| ≤ 80°

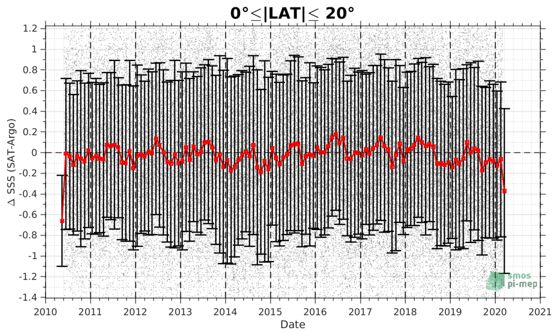

(b) 0° ≤ |LAT| ≤ 20°

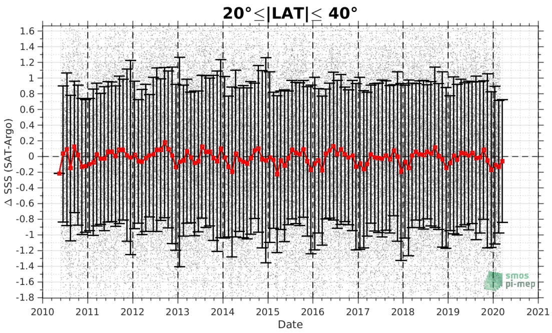

(c) 20° ≤ |LAT| ≤ 40°

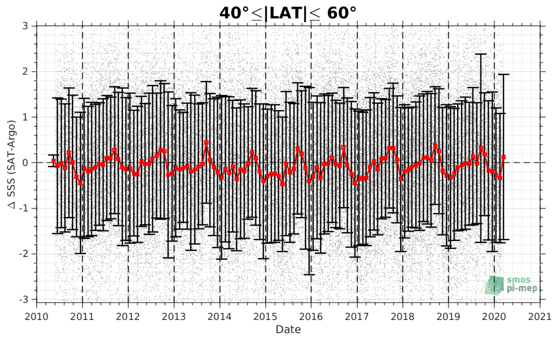

(d) 40° ≤ |LAT| ≤ 60°

Figure 20: Monthly median (red curves) of ΔSSS (Satellite - Argo) and ±1 Std (black vertical thick bars) as function of time for all the collected Pi-MEP match-up pairs estimated over the Global Ocean Pi-MEP region and for the full satellite product period are shown for different latitude bands: (a) 80°S-80°N, (b) 20°S-20°N, (c) 40°S-20°S and 20°N-40°N and (d) 60°S-40°S and 40°N-60°N.

3.6 ΔSSS sorted as function of geophysical parameters

In Figure 21, we classify the match-up differences ΔSSS (Satellite - *in situ*) between SMOS-L2-DPGS-v662 and Argo SSS as function of the geophysical conditions at match-up points. The mean and std of ΔSSS (Satellite - Argo) is thus evaluated as function of the

- *in situ* SSS values per bins of width 0.2,
- *in situ* SST values per bins of width 1°C,
- ASCAT daily wind values per bins of width 1 m/s,
- CMORPH 3-hourly rain rates per bins of width 1 mm/h, and,
- distance to coasts per bins of width 50 km.

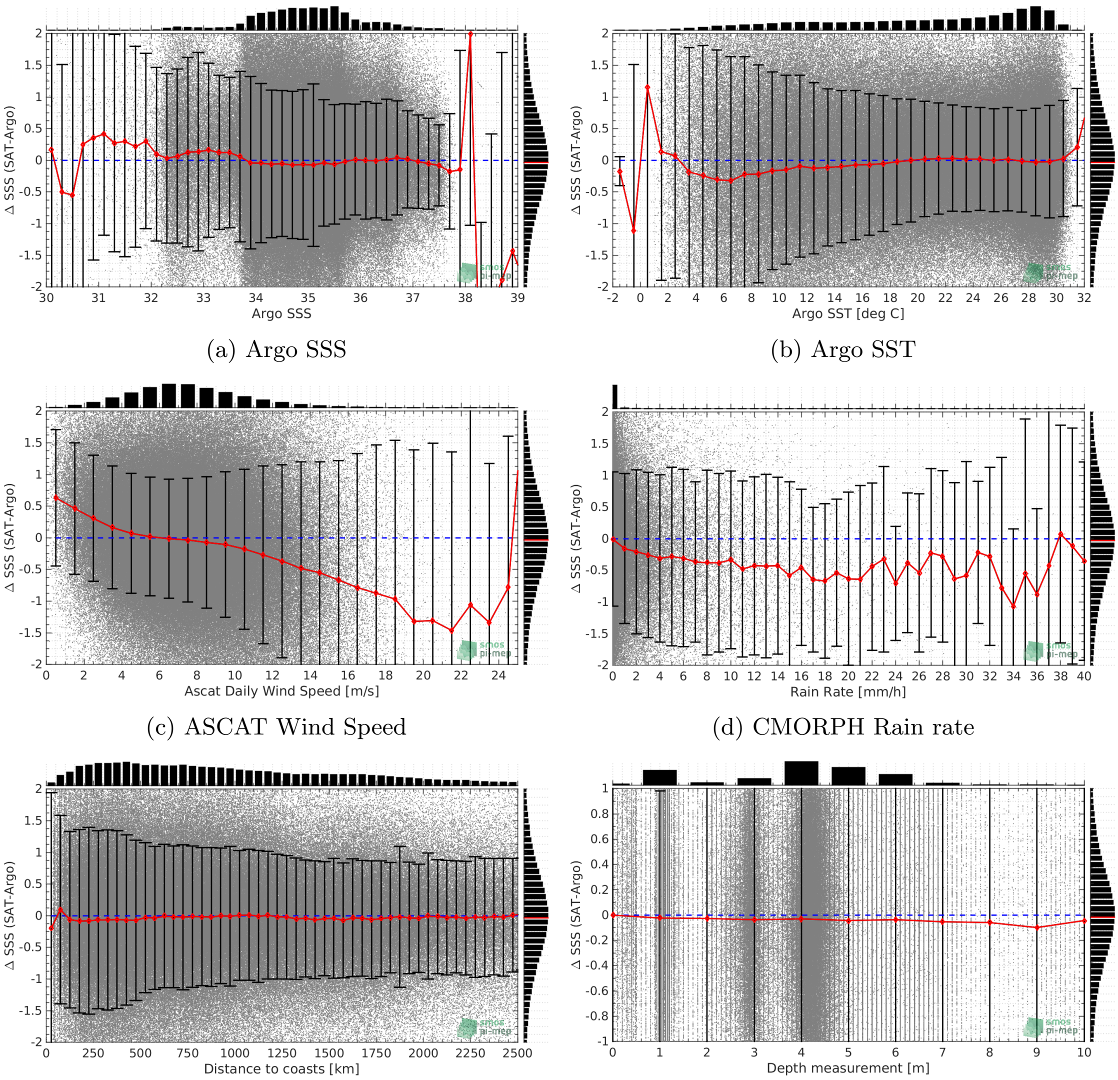

(a) Argo SSS

(b) Argo SST

(c) ASCAT Wind Speed

(d) CMORPH Rain rate

(e) Distance to coast

(f) *In situ* measurement Depth

Figure 21: ΔSSS (Satellite - Argo) sorted as function of Argo SSS values a), Argo SST b), ASCAT Wind speed c), CMORPH rain rate d), distance to coast (e) and *in situ* measurement depth (f). In all plots the median and Std of ΔSSS for each bin is indicated by the red curves and black vertical thick bars (±1 Std)

3.7 ΔSSS maps and statistics for different geophysical conditions

In Figures 22 and 23, we focus on sub-datasets of the match-up differences ΔSSS (Satellite - *in situ*) between SMOS-L2-DPGS-v662 and Argo for the following specific geophysical conditions:

- **C1**:if the local value at *in situ* location of estimated rain rate is zero, mean daily wind is in the range [3, 12] m/s, the SST is > 5°C and distance to coast is > 800 km.
- **C2**:if the local value at *in situ* location of estimated rain rate is zero, mean daily wind is in the range [3, 12] m/s.

- **C3**:if the local value at *in situ* location of estimated rain rate is high (ie. > 1 mm/h) and mean daily wind is low (ie. < 4 m/s).
- **C4**:if the mixed layer is shallow with depth <20m.
- **C5**:if the *in situ* data is located where the climatological SSS standard deviation is low (ie. above < 0.2).
- **C6**:if the *in situ* data is located where the climatological SSS standard deviation is high (ie. above > 0.2).

For each of these conditions, the temporal mean (gridded over spatial boxes of size 1°x1°) and the histogram of the difference ΔSSS (Satellite - *in situ*) are presented.

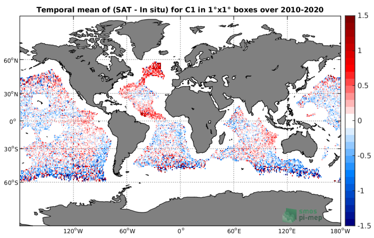

(a) RR=0 mm/h, 3< U_{10} <12 m/s, SST>5°C, distance to coast > 800 km

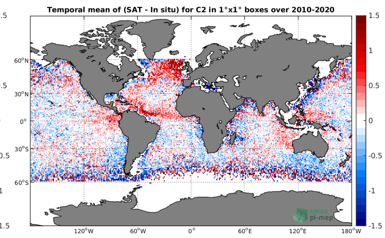

(b) RR=0 mm/h, 3< U_{10} <12 m/s

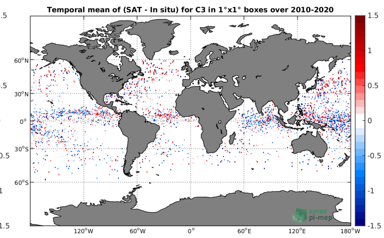

(c) RR>1mm/h and U_{10} <4m/s

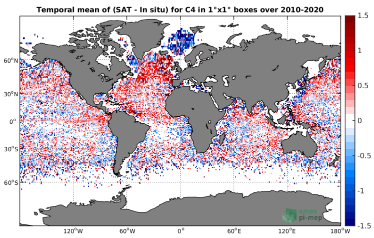

(d) MLD<20m

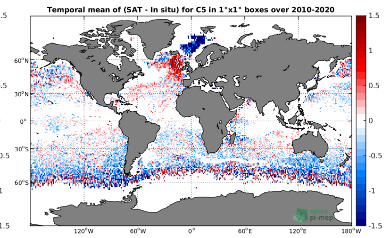

(e) WOA2013 SSS Std<0.2

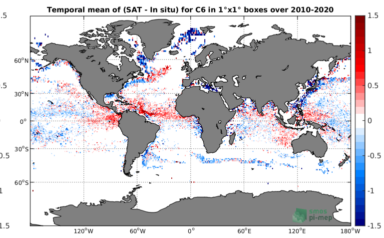

(f) WOA2013 SSS Std>0.2

Figure 22: Temporal mean gridded over spatial boxes of size 1°x1° of ΔSSS (SMOS-L2-DPGS-v662 - Argo) for 6 different subdatasets corresponding to:RR=0 mm/h, 3< U_{10} <12 m/s, SST>5°C, distance to coast > 800 km (a), RR=0 mm/h, 3< U_{10} <12 m/s (b), RR>1mm/h and U_{10} <4m/s (c),MLD<20m (d),WOA2013 SSS Std<0.2 (e),WOA2013 SSS Std>0.2 (f).

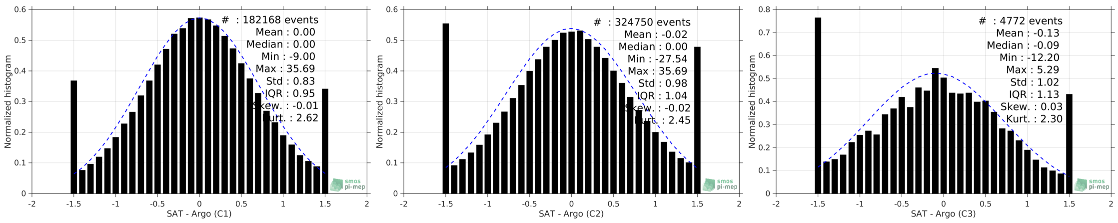

(a) RR=0 mm/h, 3< U_{10} <12 m/s, SST>5°C, distance to coast > 800 km (b) RR=0 mm/h, 3< U_{10} <12 m/s (c) RR>1mm/h and U_{10} <4m/s

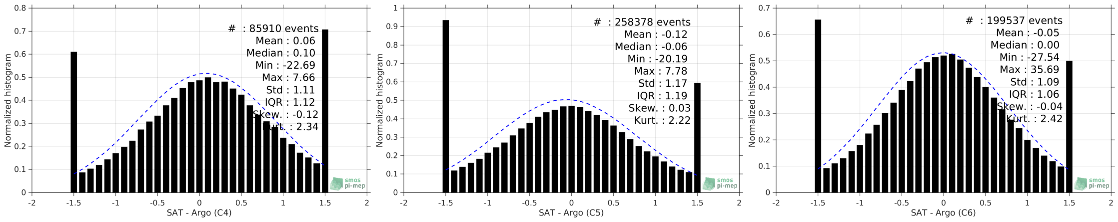

(d) MLD<20m (e) WOA2013 SSS Std<0.2 (f) WOA2013 SSS Std>0.2

Figure 23: Normalized histogram of ΔSSS (SMOS-L2-DPGS-v662 - Argo) for 6 different sub-datasets corresponding to: RR=0 mm/h, 3< U_{10} <12 m/s, SST>5°C, distance to coast > 800 km (a), RR=0 mm/h, 3< U_{10} <12 m/s (b), RR>1mm/h and U_{10} <4m/s (c), MLD<20m (d), WOA2013 SSS Std<0.2 (e), WOA2013 SSS Std>0.2 (f).

4 Summary

▶ Table 1 shows the mean, median, standard deviation (Std), root mean square (RMS), interquartile range (IQR), correlation coefficient (r^2) and robust standard deviation (Std*) of the match-up differences ΔSSS (Satellite - *in situ*) between SMOS-L2-DPGS-v662 and Argo derived over the Global Ocean Pi-MEP region and for the full satellite product period and for the following conditions:

- all: All the match-up pairs satellite/*in situ* SSS are used to derive the statistics
- C1: only pairs where RR=0 mm/h, 3< U_{10} <12 m/s, SST>5°C, distance to coast > 800 km
- C2: only pairs where RR=0 mm/h, 3< U_{10} <12 m/s
- C3: only pairs where RR>1mm/h and U_{10} <4m/s
- C4: only pairs where MLD<20m
- C5: only pairs where WOA2013 SSS Std<0.2
- C6: only pairs at WOA2013 SSS Std>0.2
- C7a: only pairs where distance to coast is < 150 km.
- C7b: only pairs where distance to coast is in the range [150, 800] km.
- C7c: only pairs where distance to coast is > 800 km.
- C8a: only pairs where *in situ* SST is < 5°C.

- C8b: only pairs where *in situ* SST is in the range [5, 15]°C.
- C8c: only pairs where *in situ* SST is > 15°C.
- C9a: only pairs where *in situ* SSS is < 33.
- C9b: only pairs where *in situ* SSS is in the range [33, 37].
- C9c: only pairs where *in situ* SSS is > 37.

Table 1: Statistics of ΔSSS (Satellite - Argo)

Condition	#	Median	Mean	Std	RMS	IQR	r^2	Std*
all	463159	-0.03	-0.09	1.14	1.14	1.13	0.45	0.85
C1	182168	0.00	0.00	0.83	0.83	0.95	0.56	0.71
C2	324750	0.00	-0.02	0.98	0.98	1.04	0.52	0.78
C3	4772	-0.09	-0.13	1.02	1.03	1.13	0.44	0.85
C4	85910	0.10	0.06	1.11	1.11	1.12	0.54	0.84
C5	258378	-0.06	-0.12	1.17	1.18	1.19	0.46	0.89
C6	199537	0.00	-0.05	1.09	1.09	1.06	0.45	0.79
C7a	18361	-0.01	-0.12	1.53	1.54	1.47	0.41	1.10
C7b	186415	-0.05	-0.13	1.29	1.30	1.26	0.42	0.94
C7c	257982	-0.02	-0.06	0.98	0.98	1.04	0.50	0.77
C8a	11691	-0.13	-0.29	2.01	2.03	2.31	0.05	1.71
C8b	112591	-0.15	-0.25	1.56	1.58	1.70	0.20	1.27
C8c	338672	-0.01	-0.03	0.90	0.90	0.99	0.53	0.74
C9a	21282	0.11	0.01	1.56	1.56	1.61	0.14	1.19
C9b	430473	-0.03	-0.09	1.12	1.12	1.13	0.36	0.84
C9c	11404	-0.07	-0.11	0.96	0.97	0.89	0.00	0.67

► Table 2 presents statistics of ΔSSS (Satellite - Argo) using Argo delayed mode only.

Table 2: Statistics of ΔSSS (Satellite - Argo) - Delayed mode

Condition	#	Median	Mean	Std	RMS	IQR	r^2	Std*
all	297211	-0.03	-0.09	1.09	1.10	1.12	0.43	0.83
C1	121710	0.00	-0.01	0.82	0.82	0.95	0.54	0.71
C2	209232	0.00	-0.02	0.94	0.94	1.03	0.51	0.77
C3	2820	-0.09	-0.13	0.98	0.99	1.14	0.45	0.85
C4	51495	0.09	0.07	1.03	1.04	1.08	0.52	0.81
C5	173380	-0.07	-0.13	1.15	1.16	1.19	0.43	0.89
C6	120235	0.01	-0.03	1.00	1.00	1.02	0.45	0.76
C7a	10168	0.01	-0.07	1.45	1.45	1.40	0.29	1.05
C7b	113850	-0.05	-0.12	1.22	1.23	1.22	0.40	0.91
C7c	172919	-0.03	-0.06	0.97	0.97	1.04	0.48	0.78
C8a	7133	-0.11	-0.26	1.96	1.98	2.25	0.01	1.68
C8b	76689	-0.16	-0.25	1.49	1.51	1.67	0.18	1.24
C8c	213369	0.00	-0.02	0.85	0.85	0.97	0.52	0.72
C9a	10821	0.14	0.05	1.42	1.42	1.56	0.04	1.16
C9b	281096	-0.04	-0.09	1.08	1.09	1.11	0.36	0.83
C9c	5294	-0.04	-0.06	0.86	0.86	0.86	0.00	0.65

▶ Table 3 presents statistics of ΔSSS (Satellite - ISAS) using only ISAS SSS values with PCTVAR<80%.

Table 3: Statistics of ΔSSS (Satellite - ISAS)

Condition	#	Median	Mean	Std	RMS	IQR	r^2	Std*
all	451195	-0.03	-0.09	1.13	1.14	1.14	0.45	0.85
C1	178113	0.01	0.00	0.82	0.82	0.96	0.57	0.72
C2	317172	0.00	-0.02	0.98	0.98	1.05	0.52	0.79
C3	4678	-0.12	-0.16	1.03	1.04	1.16	0.43	0.87
C4	83620	0.07	0.03	1.11	1.11	1.15	0.51	0.86
C5	251967	-0.06	-0.12	1.17	1.17	1.19	0.46	0.89
C6	194908	0.00	-0.04	1.08	1.08	1.08	0.44	0.81
C7a	17665	-0.02	-0.12	1.53	1.54	1.50	0.34	1.12
C7b	181572	-0.04	-0.12	1.29	1.29	1.28	0.41	0.95
C7c	251943	-0.02	-0.06	0.97	0.97	1.04	0.51	0.78
C8a	11117	-0.13	-0.29	1.99	2.01	2.32	0.04	1.71
C8b	109701	-0.16	-0.26	1.54	1.56	1.70	0.21	1.26
C8c	330174	0.00	-0.02	0.90	0.91	1.00	0.51	0.75
C9a	20577	0.01	-0.08	1.48	1.49	1.63	0.08	1.21
C9b	419457	-0.03	-0.09	1.12	1.12	1.13	0.36	0.85
C9c	11161	-0.03	-0.08	0.97	0.97	0.91	0.00	0.68

▶ Numerical values can be downloaded as csv files for Table 1, Table 2 and Table 3.

References

Argo. Argo float data and metadata from Global Data Assembly Centre (Argo GDAC), 2000. doi: 10.17882/42182.

Abderrahim Bentamy and Denis Croize Fillon. Gridded surface wind fields from Metop/ASCAT measurements. *Int. J. Remote Sens.*, 33(6):1729–1754, March 2012. ISSN 1366-5901. doi: 10.1080/01431161.2011.600348.

Abderrahim Bentamy, Semyon A. Grodsky, James A. Carton, Denis Croizé-Fillon, and Bertrand Chapron. Matching ASCAT and QuikSCAT winds. *J. Geophys. Res.*, 117(C2), February 2012. ISSN 0148-0227. doi: 10.1029/2011JC007479. C02011.

Jaqueline Boutin, Y. Chao, W. E. Asher, T. Delcroix, R. Drucker, K. Drushka, N. Kolodziejczyk, T. Lee, N. Reul, G. Reverdin, J. Schanze, A. Soloviev, L. Yu, J. Anderson, L. Brucker, E. Dinnat, A. S. Garcia, W. L. Jones, C. Maes, T. Meissner, W. Tang, N. Vinogradova, and B. Ward. Satellite and In Situ Salinity: Understanding Near-Surface Stratification and Sub-footprint Variability. *Bull. Am. Meterol. Soc.*, 97(8):1391–1407, 2016. ISSN 1520-0477. doi: 10.1175/bams-d-15-00032.1.

Clément de Boyer Montégut, Gurvan Madec, A. S. Fischer, A. Lazar, and D. Ludicone. Mixed layer depth over the global ocean: An examination of profile data and a profile-based climatology. *J. Geophys. Res.*, 109(C12), December 2004. doi: 10.1029/2004jc002378.

Clément de Boyer Montégut, Juliette Mignot, Alban Lazar, and Sophie Cravatte. Control of salinity on the mixed layer depth in the world ocean: 1. General description. *J. Geophys. Res.*, 112(C6), June 2007. ISSN 0148-0227. doi: 10.1029/2006jc003953.

Ralph R. Ferraro. SSM/I derived global rainfall estimates for climatological applications. *J. Geophys. Res.*, 102(D14):16715–16736, 07 1997. doi: 10.1029/97JD01210.

Ralph R. Ferraro, Fuzhong Weng, Norman C. Grody, and Limin Zhao. Precipitation characteristics over land from the NOAA-15 AMSU sensor. *Geophys. Res. Lett.*, 27(17):2669–2672, 2000. doi: 10.1029/2000GL011665.

Fabienne Gaillard, E. Autret, V. Thierry, P. Galaup, C. Coatanoan, and T. Loubrieu. Quality Control of Large Argo Datasets. *J. Atmos. Oceanic Technol.*, 26(2):337–351, 2009. doi: 10.1175/2008JTECHO552.1.

Fabienne Gaillard, Thierry Reynaud, Virginie Thierry, Nicolas Kolodziejczyk, and Karina von Schuckmann. In Situ-Based Reanalysis of the Global Ocean Temperature and Salinity with ISAS: Variability of the Heat Content and Steric Height. *J. Clim.*, 29(4):1305–1323, February 2016. ISSN 1520-0442. doi: 10.1175/jcli-d-15-0028.1.

Robert J. Joyce, John E. Janowiak, Phillip A. Arkin, and Pingping Xie. CMORPH: A Method that Produces Global Precipitation Estimates from Passive Microwave and Infrared Data at High Spatial and Temporal Resolution. *J. Hydrometeorol.*, 5(3):487–503, June 2004. doi: 10.1175/1525-7541(2004)005⟨0487:camtpg⟩2.0.co;2.

Nicolas Kolodziejczyk, Gilles Reverdin, and Alban Lazar. Interannual Variability of the Mixed Layer Winter Convection and Spice Injection in the Eastern Subtropical North Atlantic. *J. Phys. Oceanogr.*, 45(2):504–525, Feb 2015. ISSN 1520-0485. doi: 10.1175/jpo-d-14-0042.1.

Christian Kummerow, Y. Hong, W. S. Olson, S. Yang, R. F. Adler, J. McCollum, R. Ferraro, G. Petty, D-B. Shin, and T. T. Wilheit. The Evolution of the Goddard Profiling Algorithm (GPROF) for Rainfall Estimation from Passive Microwave Sensors. *J. Appl. Meteorol.*, 40(11): 1801–1820, 2001. doi: 10.1175/1520-0450(2001)040⟨1801:TEOTGP⟩2.0.CO;2.